Variation in a pleiotropic regulatory module drives evolution of head shape and eye size in *Drosophila*

Buchberger, Elisa[1]; Bilen, Anıl[1]; Ayaz, Sanem[1]; Salamanca, David[1,2]; Matas de las Heras, Cristina[1]; Niksic, Armin[1]; Almudi, Isabel[3]; Torres-Oliva, Montserrat[1,4]; Casares, Fernando[3]; Posnien, Nico[1,*]

[1] University Göttingen, Department of Developmental Biology, Justus-von-Liebig-Weg 11, 37077 Göttingen, Germany

[2] current address: Department of Integrative Zoology, University of Vienna, Althanstraße 14, 1090 Vienna, Austria

[3] CABD (CSIC/UPO/JA), DMC2 Unit, Pablo de Olavide University campus, Ctra. Utrera km1, 41013 Seville, Spain

[4] current address: Institute of Clinical Molecular Biology, Christian-Albrechts-University of Kiel, University Hospital Schleswig-Holstein, Kiel, Germany

*correspondence: nposnie@gwdg.de

Abstract

The size and shape of an organism is tightly controlled during embryonic and postembryonic development to ensure proper functionality. However, in the light of the breath-taking diversity of body forms observed in nature, developmental processes must have evolved to allow evolutionary changes in adult morphology. Therefore, gene regulatory networks (GRNs) that orchestrate organ development are mostly constrained, but nodes and edges within such networks must change to give rise to morphological divergence. Identifying such tuning nodes remains a major challenge in evolutionary developmental biology. Here, we combined comparative transcriptomics and chromatin accessibility data to study developmental differences leading to natural variation in compound eye size and head shape in the two closely related *Drosophila* species *D. melanogaster* and *D. mauritiana*. We show that variation in expression of the GATA transcription factor Pannier (Pnr) is associated with extensive remodeling of the transcriptomic landscape during head development. Since U-shaped (Ush), a co-factor of Pnr, is involved in the same regulatory context, we argue that variation in expression of both factors may be a driver of divergence in head morphology. Applying functional genetics and geometric morphometrics we confirmed that manipulation of *pnr* expression in *D. melanogaster* largely phenocopies *D. mauritiana* dorsal head shape and ommatidia number. Therefore, we propose that the regulatory module composed of Pnr and Ush represents a tuning node within the otherwise highly conserved GRN underlying head development in *Drosophila*.

Introduction

The morphological diversity present in nature is a key prerequisite for organisms to adapt to an ever-changing environment. One of the major goals in biological research is to unravel the internal and external forces shaping this morphological variability. Since the genome of an organism contains instructive information about its morphology, it is important to establish genotype-phenotype correlations for a given morphological trait [1,2]. The genetic architecture of relatively simple traits has been successfully determined at a high resolution. For instance, natural variation in body pigmentation in the vinegar fly *Drosophila melanogaster* and the beach mouse *Peromyscus polionotus* has been mapped to individual nucleotides affecting gene expression [3,4] or protein function [5], respectively. Also, the genetic basis of the gain or loss of structures like trichomes in *Drosophila* [6], armor plates in three spine stickleback fish [7] or the repeated loss of eyes in cave fish [8,9] has been successfully revealed. However, the genetic changes underlying the evolution of complex traits, such as the size and shape of organs remain largely elusive to date.

The size and shape of an organ is defined during embryonic and post-embryonic development relying on the correct activation and repression of developmental genes, which are orchestrated by a complex interplay between gene products in developmental gene regulatory networks (GRNs) [10]. Developmental processes [11,12] and the expression of genes regulating them [13–15] tend to be robust against genetic or environmental perturbations. This is best exemplified by the observation that the individual loss of function of many genes in yeast [16] and the nematode *Caenorhabditis elegans* [17] rarely has deleterious effects for the organism, suggesting that such changes are buffered by the underlying GRNs. It has been demonstrated that robustness is often the result of redundancies [18], either on the level of *cis*-regulatory elements [19,20] or transcription factors and signaling molecules [21,22]. While the robustness of developmental GRNs ensures the formation of functional organs, some degree of flexibility in the network architecture is necessary to allow changes in size and shape of a certain organ to occur throughout evolution. Therefore, we propose that developmental GRNs must contain at least two types of nodes (i.e. genes): structural nodes and tuning nodes. Structural nodes confer phenotypic stability because variation in such nodes (e.g. variation in expression of the gene) is either prevented by tight regulation at the locus or buffered downstream in the GRN. In contrast, tuning nodes represent genes for which variation is tolerated within the GRN and results in quantitative phenotypic variation. Therefore, revealing structural and tuning nodes in

developmental GRNs allows gaining new insights into constrained and variable developmental processes, respectively.

One approach to reveal tuning nodes is first to identify genetic variants associated with morphological diversity and then in a second step to establish regulatory interactions of genes affected by those variants. However, variation in complex morphological traits is influenced by many genetic loci with small effect sizes, which are spread throughout various genomic locations [23–25]. For instance, mandible and craniofacial shape differences between mouse strains are influenced by various loci located on most of the chromosomes [26–29]. Similarly, studies in *Drosophila* revealed that loci on several chromosomes contribute to differences in eye size and head shape [30–32]. These examples corroborate the complexity of the genetic architecture of such traits and highlight the difficulty to determine individual causative molecular changes.

As an alternative, we propose to first identify tuning nodes within the GRN governing the development of a variable morphological trait. We assume that variation in the expression or function of putative tuning nodes (e.g. genes coding for transcription factors) directly affects the expression of downstream target genes (i.e. "gene modules" [33]). Candidate tuning nodes can then be validated, for instance, by functionally testing whether quantitative differences in their expression levels indeed affect the phenotypic outcome. As a model we compared genome wide patterns of gene expression during eye and head development in the two closely related *Drosophila* species *D. melanogaster* and *D. mauritiana*, which vary in adult eye size and head shape [32,34,35]. Specifically, *D. mauritiana* develops larger compound eyes with more ommatidia, especially in the dorsal eye. The bigger eyes of *D. mauritiana* are accompanied by a narrower interstitial head cuticle [34], recapitulating the common origin of eye and head cuticle tissue from the same eye-antennal imaginal disc during larval development [36]. Since the GRN governing eye-antennal disc development is well understood in *D. melanogaster* [37–40], this process represents an excellent model to link morphological diversity to developmental and genetic variation.

Here we combined comparative transcriptomics and chromatin accessibility data for different developmental stages of head development in *D. melanogaster* and *D. mauritiana* to reveal tuning nodes in an otherwise largely conserved GRN. A systematic co-expression and transcription factor enrichment analysis suggested that many differentially expressed genes

were regulated by the GATA transcription factor Pannier (Pnr). We found evidence that Pnr activates and represses its target genes during head development and we propose that this dual role is facilitated by its co-factor U-shaped (Ush) since both factors are involved in the same regulatory context. Applying functional genetics and geometric morphometrics, we confirmed that the overexpression of *pnr* in *D. melanogaster* indeed phenocopies aspects of the *D. mauritiana* head shape and eye size.

Results

D. melanogaster and *D. mauritiana* exhibit differences in dorsal head shape

To reveal tuning nodes within GRNs the development of a variable morphological structure must be studied. *Drosophila* eye size and head shape represent such traits since they vary extensively between *D. melanogaster* and *D. mauritiana* with the latter having bigger eyes due to more ommatidia at the expense of interstitial face cuticle [30,34,35]. Since eye size differences are most pronounced in the dorsal part [34], we proposed that the shape of the dorsal interstitial cuticle may vary as well. To test this hypothesis, we comprehensively quantified differences in the dorsal head morphology among the two sister species.

We placed 57 landmarks on pictures of dorsal heads and applied a geometric morphometrics analysis (Figure 1a). A discriminate function analysis clearly distinguished the head shapes of *D. melanogaster* and *D. mauritiana* (Figure 1b) (p-value= 0.0001). In accordance with previous data [34], we found main differences in dorsal eye size with the eye area protruding more towards the back of the head in *D. mauritiana* (Figure 1b). The posterior expansion of the eye area in *D. mauritiana* was accompanied by a narrower dorsal head region, which affected both the orbital cuticle and the dorsal frons region. The ocellar complex was slightly shifted ventrally in *D. mauritiana* (Figure 1b). In summary, we found that *D. melanogaster* and *D. mauritiana* do not only differ in the size of dorsal eye, but they also exhibit variation in the relative contribution of different head regions to the dorsal head capsule.

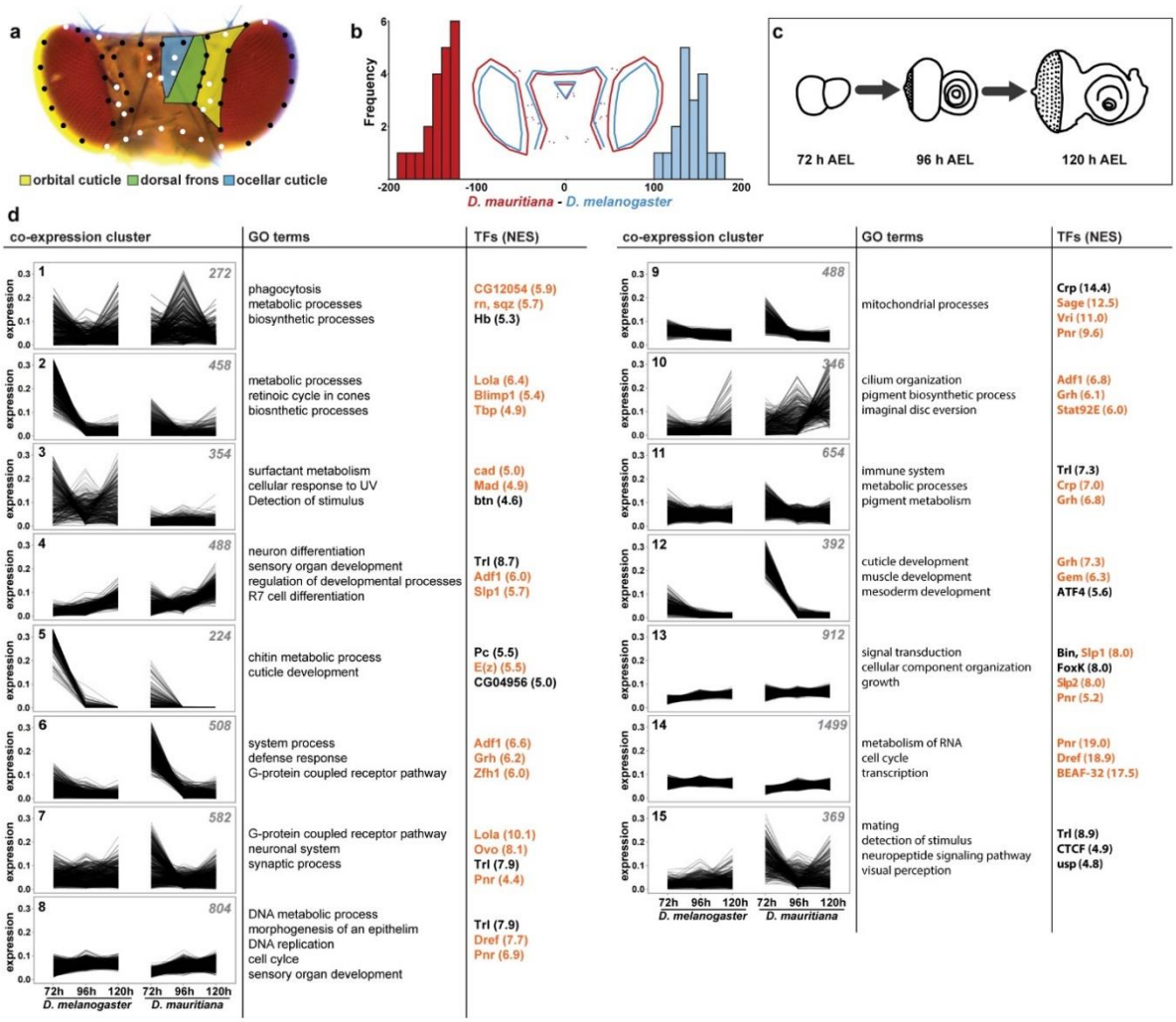

Figure 1 | Quantitative differences in dorsal head shape are associated with extensive remodeling of the transcriptome underlying eye-antennal disc development. a, Dorsal view of a *Drosophila melanogaster* head. The head cuticle consists of three morphologically distinguishable regions, namely the orbital cuticle (yellow) next to the compound eye, the dorsal frons (green) and the ocellary cuticle (blue). The 57 landmarks that were used to analyze head shape are shown as fixed (white) and sliding landmarks (black). **b,** Discriminant function analysis distinguishes mean dorsal head shapes of *D. melanogaster* (blue) and *D. mauritiana* (red). Difference between means: Procrustes distance: 0.094, p-value= 0.0001 **c,** Transcriptomic datasets were generated for developing eye-antennal discs for both species at three developmental stages: 72h after egg laying (AEL; late L2), 96h AEL (mid L3) and 120h AEL (late L3). **d,** Cluster analysis of all differentially expressed genes between *D. melanogaster* and *D. mauritiana*. The number of genes in each cluster is given in the upper right corner. Significantly enriched GO terms are provided for each cluster. TFs refer to potential upstream regulators and the respective NES values (non-redundant occurrence and excluding non-*Drosophila* motifs). Factors written in orange are significantly differentially expressed in at least one stage between the two species. A complete list of enriched GO-terms and potential upstream factors is available in Table S2.

Morphological differences between *D. melanogaster* and *D. mauritiana* are associated with variation in the developmental transcriptomic landscape

To understand the developmental basis of the size and shape differences in dorsal head structures (Figure 1b), we obtained comparative transcriptomes for eye-antennal disc development. Since we found that the retinal region (Supplementary Figure 1a and b) and the anlagen of the interstitial cuticle (Supplementary Figure 1c) started to show differences

between *D. melanogaster* and *D. mauritiana* discs at 96 h AEL, we chose to sequence three stages representing the onset (72 h AEL), progression (96 h AEL) and termination of differentiation (120 h AEL) (Figure 1c and Supplementary Figure 2) [41]. The GRN governing eye-antennal disc development must be composed of structural nodes that are crucial to ensure proper eye and head formation. Therefore, we first confirmed that genes with stable expression between species represent central processes involved in eye-antennal disc development (Supplementary Figure 3).

To test whether differences in adult head morphology are associated with variation in the transcriptomic landscape during eye-antennal disc development, we next analysed those genes that were differentially expressed between species. 72 % of variation in the dataset was due to differences between 72h and the other two stages (Supplementary Figure 4), an observation that was confirmed by a pairwise differential expression analysis. With 6,683 genes, we found the highest number of differentially expressed genes (DEGs) at 72 h AEL, while only 3,260 and 2,380 genes were differentially expressed at 96h AEL and 120 h AEL, respectively. Differential expression was not biased towards one species since we observed an equal number of DEGs with higher expression in *D. melanogaster* and *D. mauritiana*, respectively (Supplementary Table 1). Clustering of DEGs based on temporal expression profiles revealed highly variable expression dynamics between species (Figure 1d).

To identify putative developmental processes affected by the interspecific differences in the transcriptomic landscape, we searched for enriched GO categories associated with each gene cluster. Genes involved in generic metabolic and energy related processes were enriched in various clusters including those with dynamic (Figure 1d, e.g. cluster 1 and 2) as well as stable temporal expression (Figure 1d, e.g. cluster 11). Genes that tended to be highly expressed at later stages were enriched for factors regulating neuronal differentiation processes (Figure 1d, e.g. cluster 4) and in clusters with stably expressed genes, we observed an enrichment for cell cycle control and tissue growth (Figure 1d, e.g. clusters 8 and 14). In summary, we revealed extensive variation in the transcriptomic landscape of developing eye-antennal discs between *D. melanogaster* and *D. mauritiana* with different processes being affected by these changes.

Variation in the transcriptomics landscape is caused by variation in expression of upstream regulators

The observed interspecific differences in gene expression dynamics must be the result of variation in the underlying regulatory interactions. Therefore, we treated the DEGs with similar expression profiles (i.e. clusters in Figure 1d) as "gene modules" [33] that are regulated by similar transcription factors (i.e. putative tuning nodes in the developmental GRN). To identify such transcription factors, we searched in stage-specific open chromatin regions for enriched transcription factor binding motifs for each co-expression cluster (see Materials and Methods and Supplementary Figure 2 for details). Each cluster showed enrichment of motifs for a unique combination of transcription factors, suggesting that the variation in gene expression profiles is due to differences in different regulatory interactions.

Differential gene expression can be the result of differences in the expression of their regulating transcription factors. Indeed, we found that ~61% (92 of 150) of the putative upstream transcription factors (NES > 4.0) were differentially expressed at least at one developmental stage (False discovery rate (FDR) 0.05) (Figure 1d and Supplementary Table 2). Those transcription factors which are differentially expressed and regulate genes with expression differences between species are prime candidates to be putative tuning nodes in the GRN underlying eye-antennal disc development. Some of the identified transcription factors have previously been described to be involved in eye-antennal disc development, suggesting that variation in their expression may indeed affect eye and head development. For instance, Lola (Figure 1d; clusters 2, 5, 7 and 12) regulates ocelli [42] and photoreceptor and cone cell development [43], Blimp-1 (Figure 1d; cluster 2) controls the progression of retinal differentiation [44,45] and Mad (Figure 1d; clusters 3, 4 and 15), the transcription factor that mediates Decapentaplegic (Dpp) – signalling [46], is involved in various processes in the eye-antennal disc [47–49]. Additionally, in 5 of 15 clusters (NES > 4) (Figure 1d; e.g. clusters 7-9, 13 and 14) (in 9 of 15 clusters, NES > 3) we found a strong enrichment of motifs predicted to be bound by the GATA transcription factor Pnr, which is for instance involved in establishing the early dorsal ventral axis of the eye [50–52]. In summary, through co-expressed "gene modules" we identified putative tuning nodes whose differential expression had a major impact on the transcriptomic landscape of developing eye-antennal discs among species.

Pannier and U-shaped are active in the same regulatory network to regulate differentially expressed genes

Variation in gene expression often does not result in phenotypic differences because they are buffered in GRNs [21,53,54]. Therefore, it remains questionable, whether the putative tuning nodes are indeed relevant for the differences in head morphology between *D. melanogaster* and *D. mauritiana*. To test this, we further investigated the role of Pnr, which is an interesting candidate transcription factor for the following reasons: 1. Our global clustering and motif enrichment analyses suggest that Pnr regulates many DEGs between both species (Figure 1d). 2. *pnr* itself is differentially expressed between *D. melanogaster* and *D. mauritiana*, with higher expression in the latter species (Figure 2a). 3. Pnr is known to be expressed in the dorsal portion of the eye-antennal disc [50] and it is involved in determining the dorsal-ventral axis of the retinal field in the early L2 discs [50,52,55]. Additionally, later during eye-antennal disc development, Pnr influences the ratio of retinal and head cuticle fate in the dorsal disc by repressing retinal determination genes [50,56,57].

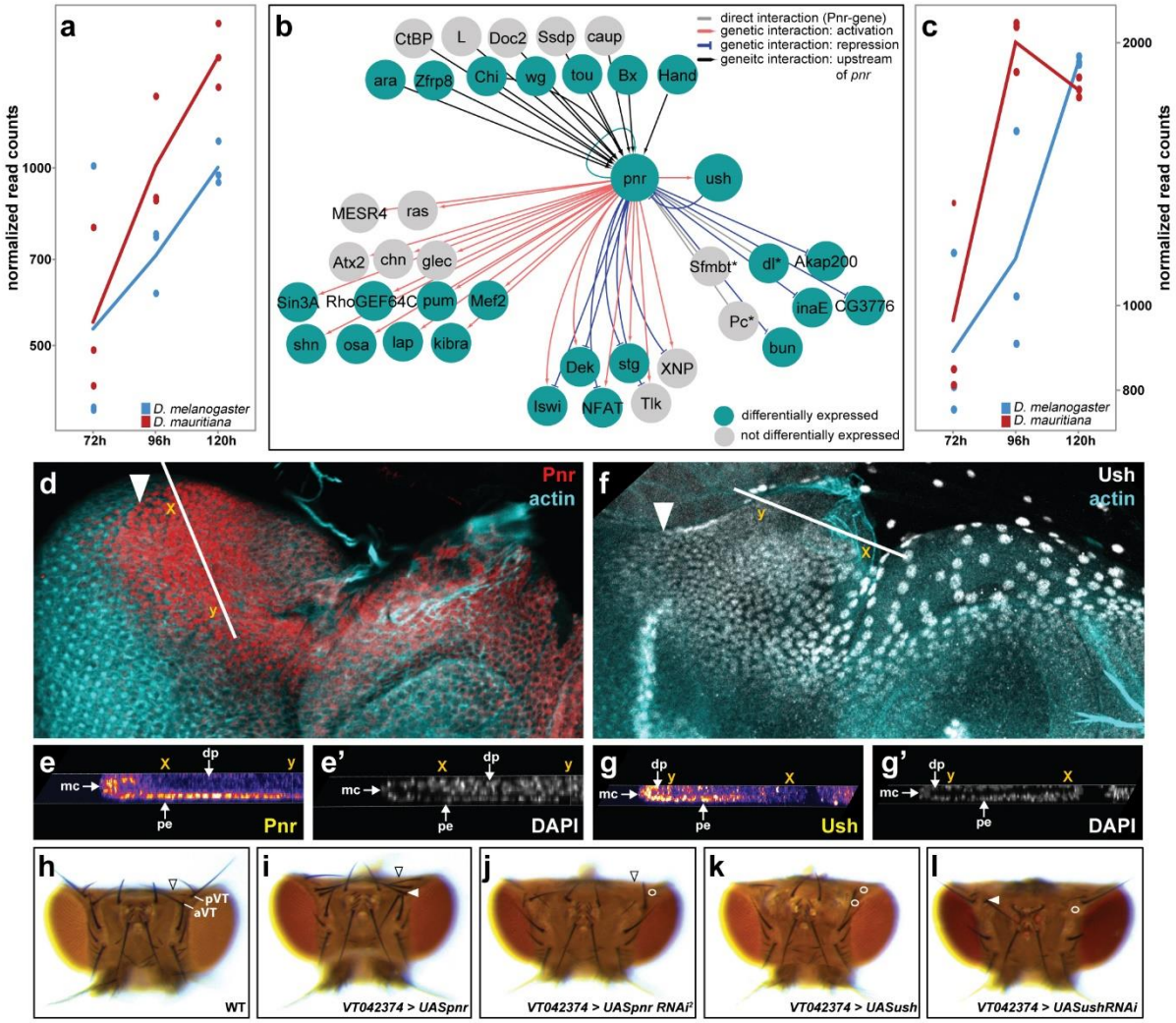

Figure 2 | Expression, regulatory interactions, and function of Pnr and Ush in head cuticle and bristle development. a, Expression dynamics of the *pnr* transcript at the three developmental stages in *D. melanogaster* (blue) and *D. mauritiana* (red) based on rlog transformed read counts. **b,** Network reconstruction of known interactions upstream and downstream of Pnr that overlap with our Pnr target gene list. 14 of the 29 target genes are activated (red edges) and 8 genes are repressed (blue edges) by Pnr. 6 target genes showed both types of interactions. 21 of the 30 putative Pnr target genes (68%) were differentially expressed (green nodes). **c,** Expression dynamics of the *ush* transcript at the three developmental stages in *D. melanogaster* (blue) and *D. mauritiana* (red) based on rlog transformed read counts. **d, e,** Pnr protein location in 3rd instar eye-antennal discs in *D. melanogaster*. The Pnr protein is present in the dorsal peripodial epithelium (pe) of the developing disc (**d**), including a few cells of the margin cells (mc) and the disc proper (dp) (**e'**). The white arrow in **d** marks the morphogenetic furrow, the solid white line marks region of the cross section shown in **e** and **e'** and the x and y coordinates indicate the same location in **d, e** and **e'**. **f, g,** Ush protein location in 3rd instar eye-antennal discs in *D. melanogaster*. The Ush protein is, similarly to Pnr (compare to **d**), expressed in the dorsal peripodial epithelium (pe) of the developing disc (**f**), including a few cells of the margin cells (mc) and the disc proper (dp) (**g'**). The white arrow in **f** marks the morphogenetic furrow, the solid white line marks region of the cross section shown in **g** and **g'** and the x and y coordinates indicate the same location in **f, g** and g'. **h,** Dorsal view of an adult wild type head of *D. melanogaster*. Posterior (pVT) and anterior vertex bristles (aVT) are labelled. The arrowhead marks the occipital region. **i,** Overexpression of *pnr* did not lead to major irregularities in the dorsal head cuticle, but to duplication of the pVT bristle next to the compound eye (white arrowhead) (N= 9 females, N=10 males). **j,** Knock-down of *pnr* resulted in visible enlargement of the occipital region (black arrowhead) and to the loss of the pVT bristle next to the compound eye (white circle) (n= 10 females, 10 males). **k,** Overexpression of *ush* resulted in irregularities in the dorsal head cuticle, and to the loss of the pVT and aVT bristles (white circles) next to the compound eye (n= 10 females). **l,** Knock-down of *ush* resulted in slight irregularities of the dorsal head cuticle, to loss (white circle) or misplacement (white arrowhead) of the aVT bristle (n= 11 females).

To learn more about the regulatory interactions of Pnr, we first refined the list of its potential target genes by searching for the Pnr-specific GATA motif in genomic regions that were accessible during eye-antennal imaginal disc development (see Materials and Methods and Supplementary Figure 2 for details). In 14,511 open chromatin regions we found 1,335 Pnr-specific GATA motifs associated with 1,060 genes expressed in our RNAseq dataset, suggesting that those genes were active during eye and head development. In the regulatory regions of the putative Pnr target genes we found a strong enrichment of Pnr binding sites (Supplementary Figure 5a) and many of the genes were also predicted to be regulated by Pnr in our cluster analysis (see Figure 1d and Supplementary Figure 5b). In line with the known functions of Pnr during eye-antennal disc development, the putative Pnr target genes were highly enriched in processes like compound eye development and growth as well as cell cycle progression (Supplementary Figure 5c). Additionally, a cross-validation of our putative Pnr target genes with the DroID interaction database [58,59] showed that our list contained three known direct target genes (i.e. Pnr-regulatory sequence interaction; *dl, Pc* and *Sfmbt*) and 23 genes with known genetic interactions (Figure 2b). 17 out of these 26 genes showed differential expression between the two species. Taken together, we identified a high confidence list of Pnr target genes during eye-antennal disc development.

Using this list, we next asked how *pnr* expression influenced the expression of its target genes. 67.5 % (716 of 1,060 genes) of the expressed target genes showed expression differences between *D. melanogaster* and *D. mauritiana* (Supplementary Table 3). Intriguingly, we found genes that are activated as well as repressed by Pnr among the differentially expressed target genes (Supplementary Figure 6 and Figure 2b), suggesting that variation in *pnr* expression affects both types of targets. Previous studies in embryos and the wing disc have shown that Pnr, which normally acts as an activator, acquires a repressive function upon heterodimerization with its co-factor U-shaped (Ush) [60–62]. Although, it was previously stated that *ush* is not expressed in the eye-antennal disc [50,61], it was expressed in all three studied stages of eye-antennal disc development in our RNAseq data (Figure 2c). Additionally, like *pnr*, *ush* expression was mostly higher in *D. mauritiana* (Figure 2c). Therefore, we hypothesized that Ush may also act as a co-factor during eye-antennal disc development alongside Pnr.

To further test this hypothesis, we first asked whether both proteins are present in the same cells of the eye-antennal disc. Using newly generated antibodies against Pnr and Ush, we detected both proteins in largely overlapping domains (Figure 2d-g and Supplementary Figure 7) in the large nuclei of the dorsal peripodial epithelium (compare Figure 2d to f) and in a subset of the cuboidal margin cells in the disc proper (compare Figure 2e to g). Lineage tracing experiments showed that descendants of *pnr*-positive cells were identified in the dorsal disc margin, in the disc proper (Supplementary Figure 8a) as well as further ventrally in the peripodial epithelium (Supplementary Figure 8b), suggesting a dynamic expression of *pnr* during eye-antennal disc development.

The co-expression suggests that both genes may be involved in similar developmental processes and that they interact genetically. Therefore, we sought to test if modulation of *pnr* and *ush* expression levels similarly affected head development. To this end, we overexpressed and knocked down both genes in the dorsal eye-antennal disc in a domain that is reminiscent of *pnr* expression (Supplementary Figure 9a,b). Successful manipulation of the expression was confirmed by reduced and enhanced protein expression in knock-down and overexpression discs, respectively (Supplementary Figure 9c-h). Upon manipulation of *pnr* and *ush* expression levels, we consistently found an effect on dorsal head cuticle development and formation of the vertical bristles (aVT and pVT) at the rim of the compound eye (Figure 2h-l). These observations are consistent with the reported role of Pnr and Ush in governing bristle pattern formation in the thorax [60,63]. Additionally, this data indicates that *ush* is not only expressed, but also functional during dorsal head development. To test for genetic interactions, we asked whether manipulation of *pnr* expression affected *ush* expression and vice versa. Due to the qualitative nature of our experimental setup we could not obtain conclusive results for some of the tested combinations. However, we observed a reduced Ush signal upon knock-down of *pnr* (Supplementary Figure 9i), suggesting a positive interaction between *pnr* and *ush*. Additionally, upregulation of *ush* resulted in slightly reduced Pnr protein levels (Supplementary Figure 9j), suggesting a negative impact of Ush on *pnr* expression. Further support for this idea comes from the induction of a double-antenna phenotype when *ush* was overexpressed using a stronger *pnr* driver line (Supplementary Figure 9k) [61], a phenotype that we also observed upon *pnr* knock-down (Supplementary Figure 9l) [50].

In summary, we could show that natural variation in *pnr* expression between *D. melanogaster* and *D. mauritiana* results in considerable remodelling of the transcriptomic landscape. We suggest a dual role of Pnr during eye-antennal disc development, which is most likely mediated by its co-factor Ush since both genes are co-expressed, interact genetically (Supplementary Figure 9m) and are involved in dorsal head development. Overall, our data suggests that interspecific variation in *pnr* expression may indeed influence dorsal head shape and eye size as observed between species.

Overexpression of *pannier* phenocopies aspects of the differences observed between *D. melanogaster* and *D. mauritiana*

To test if variation in *pnr* expression indeed has the potential to explain naturally occurring differences in eye size and head shape we quantitatively analysed the adult heads originating from gain- and loss-of-function experiments applying geometric morphometrics and ommatidia counting (see Materials and Methods for details).

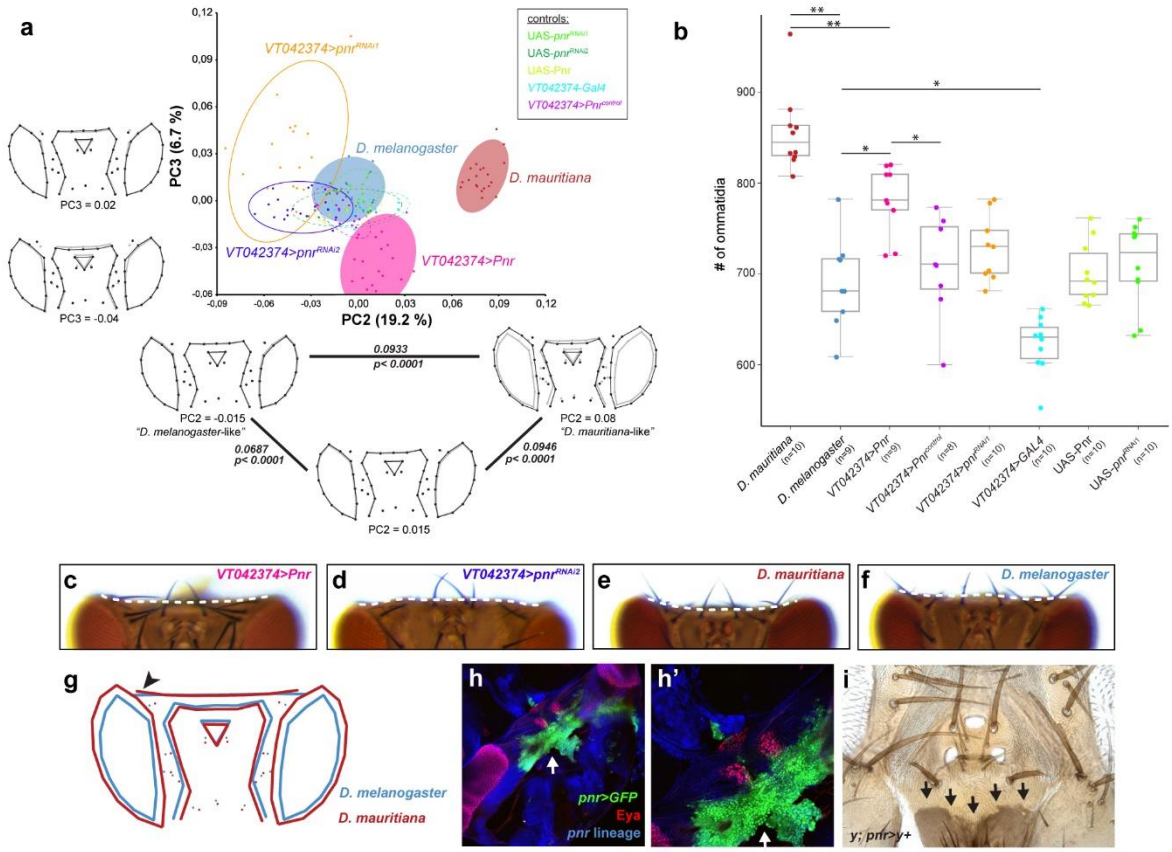

Figure 3 | Overexpression of *pnr* in *D. melanogaster* phenocopies *D. mauritiana* head shape and eye size. a, Principal component analysis of dorsal head shapes. Shape outlines for PC values are given along the PC2 and PC3 axes, respectively, as

indicated below each outline. In the triangle along PC2, the Procrustes distance between each shown shape outline is provided, as well as the p-value after permutation test with 1,000 cycles. Overexpression of *pnr* shifts the dorsal head shape towards a *D. mauritiana* head shape. **b,** Number of ommatidia counted in one compound eye per individual. The significance was calculated by ANOVA and each pairwise comparison was calculated using Tukey's HSD test; **<=0.01; *<=0.05. The color code in **a** and **b** is the same. **c,** Representative dorsal view of an adult head after overexpression of *pnr* and **d,** after knockdown of *pnr*. **e,** Representative dorsal view of an adult head *D. mauritiana*. **f,** Representative dorsal view of an adult head of *D. melanogaster*. The dotted lines in **c-f** mark the border of the occipital region. **g,** Mean shapes of *D. melanogaster* (blue) and *D. mauritiana* (red) heads after discriminant function analysis including seven additional landmarks in the occipital region. The black arrowhead marks the lateral bending of the occipital region in *D. mauritiana*. **h,** *pnr*-expression in developing pupal head structures. Cells marked with *pnr*>GFP accumulated in the future occipital region (green) behind the developing ocelli (red), and the head region where the two discs fuse (white arrow). **h',** Higher magnification of **h**. **i,** *pnr* lineage in adult dorsal heads shown by cells in which *yellow* expression is restored (black arrows).

A principal component analysis of head shape variation showed that PC2 explained 19.2% of the observed variation in head shape and PC3 explained 6.7% (Figure 3a; note that PC1 captured a technical artefact, see Supplementary Figure 10). Variation along PC2 mainly captured differences in the proportion of eye *vs.* interstitial cuticle tissue in the dorsal head, as well as the location of the ocellar region. Intriguingly, the overexpression of *pnr* in the dorsal head region resulted in a shift from a "*D. melanogaster*"-like shape towards a more "*D. mauritiana*"-like shape along PC2, with an enlargement of the eyes at the expense of a slight reduction of the interstitial cuticle (Figure 3a). Ommatidia counting in entire eyes confirmed that the increase in eye area upon *pnr* overexpression was indeed due to an increase in number of ommatidia (Figure 3b). Note that *pnr* RNAi influenced overall head shape (Figure 3a), but we could not observe an impact on the number of ommatidia (Figure 3b).

PC3 explained mostly differences in the dorsal-posterior head cuticle and the location of the ocellar region (Figure 3a). We analysed the dorsal-posterior head cuticle in more detail and observed that the occipital region was more convex upon *pnr* overexpression (Figure 3c), whereas downregulation consistently led to an enlargement of these regions (Figure 3d). Intriguingly, in accordance with a higher expression of *pnr* in *D. mauritiana,* we found a more convex occipital region in *D. mauritiana* (Figure 3e) compared to a more concave shape in *D. melanogaster* (Figure 3f, g). Detection of *pnr* expression in pupae (Figure 3h) as well as the analysis of *pnr*-expressing clones in adult heads (Figure 3i) confirmed that *pnr* was indeed expressed in the future occipital region.

In summary, we were able to phenocopy aspects of the "*D. mauritiana*"-like head shape and eye size by upregulating *pnr* expression in the developing eye-antennal disc. This data strongly suggests that natural variation in *pnr* expression can indeed contribute to phenotypic differences between species.

Discussion

The tight control of developmental processes is crucial to ensure the formation of functional organs. Accordingly, the mutation rates of central developmental regulators, such as transcription factors and signalling molecules, are low [64–66] and such factors tend to be functionally conserved across the animal kingdom [67]. Since morphological differences in adult traits result from variation in developmental processes [68–70], it has been suggested that variation in expression of functionally conserved developmental regulators is a major driver of morphological divergence [71,72]. Gene expression and therefore developmental programs are regulated by interactions of gene products in extensively wired GRNs [73,74]. Crucial nodes and connections in such GRNs must be protected against fluctuations (referred to as structural nodes) to keep the overall morphology and functionality of an organ stable throughout time. Indeed it has been shown that changes in gene function and expression are often buffered in GRNs to maintain a stable phenotypic outcome [16–22]. To reveal phenotypically relevant tuning nodes the development of an organ that exhibits quantitative differences in adult morphology must be compared. Since natural intra- and interspecific variation in head shape and eye size is pervasive among species of the *D. melanogaster* subgroup [30–32,34,35,75–77], we used the development of these adult structures from eye-antennal discs to address this question.

In accordance with overall functionally and morphologically conserved adult head shape in *D. melanogaster* and *D. mauritiana*, we found that the expression of many genes was conserved between the two species during head and compound eye development. Those genes represented key developmental and metabolic processes, suggesting that the GRNs are still very similar between these two closely related species. However, the observed quantitative interspecific differences in eye size and head shape must be due to variation in some parts of the GRN that may be selected for if it translates into phenotypic diversity that is advantageous to the organism [78–80].

Because of the regulatory interactions within GRNs, we hypothesized that tuning nodes can be elucidated by their impact on the expression of their target genes [74]. We found a significant number of the identified upstream regulators to be differentially expressed themselves, thus qualifying them as putative tuning nodes. Given the capacity of GRNs to buffer expression changes, it remains unclear whether those changes indeed result in phenotypic

differences. Since we observed variation in head morphology between *D. melanogaster* and *D. mauritiana* (this work and [34]) and identified Pnr as a putative tuning node we functionally tested whether variation in expression of this transcription factor translates into interspecific phenotypic differences. Overexpression of *pnr* in the dorsal eye-antennal disc of *D. melanogaster* phenocopied major aspects of the dorsal *D. mauritiana* head shape and eye size, showing a functional link between enhanced *pnr* expression and these morphological differences.

Intriguingly, manipulation of *pnr* expression simultaneously affected the interstitial cuticle and the compound eyes, suggesting that Pnr is involved in specifying the ratio between retinal tissue and head cuticle. Support for this observation comes from prior developmental analyses that established two major roles of Pnr during *D. melanogaster* eye-antennal disc development. 1) During early eye-antennal disc development, Pnr plays a pivotal role in defining the dorsal-ventral boundary and is therefore responsible for overall tissue growth [50,52,55]. Throughout larval development *pnr* is predominantly expressed in the dorsal peripodial epithelium and our lineage tracing experiment showed that, during earlier stages, *pnr* must be expressed in cells that contribute to the complete dorsal lineage as well as in cells of the dorsal posterior margin where the morphogenetic furrow is initiated [38]. Recent data shows that Eyeless (Ey) activity in the peripodial epithelium and the margin cells is necessary for the initiation of the morphogenetic furrow and the placement of the dorsal-ventral boundary [81]. Our result that *ey* is among the putative direct Pnr target genes, offers an exciting and yet unpredicted early role of Pnr in *ey* regulation in the peripodial epithelium and in margin cells, providing a potential functional link to this well-established early role of Pnr. 2) From the late second instar stage onwards, Pnr is involved in regulating the ratio of retinal cells *vs*. head cuticle cells by repression of members of retinal determination network [56]. With *ey* and *eyegone* (*eyg*) we found two members of the retinal determination network among the putative Pnr targets and both genes must be repressed to ensure proper dorsal interstitial cuticle development [82,83]. If Pnr is indeed involved in the regulation of these factors remains to be functionally tested. Our tracing experiment revealed that *pnr*-expressing cells contribute to the dorsal occipital head region, suggesting that a direct effect on the morphological differences in this region is very likely. The later role in defining the dorsal cuticle *vs.* retinal fate is well in line with the observed interspecific trade-off between eye size and interstitial cuticle, where the

increased eye size in *D. mauritiana* goes along with a reduction of dorsal interstitial cuticle and a convex bending of the occipital head region.

The multiple roles of Pnr during eye-antennal disc development, which are most likely facilitated by its temporally (early *vs.* late function) and spatially (expression in peripodial epithelium and in margin cells) defined expression, may explain contradicting results obtained by different functional studies. While we observed an increase in eye size upon overexpression of *pnr* in its endogenous expression domain, previous work reported dorsal retinal overgrowth and ectopic eye fields after the induction of loss of function clones using an *ey*-Gal4 driver [50,56]. Since the *ey*-Gal4 driver is active from early stages on [81], the retinal overgrowth very likely results from the induction of an ectopic dorsal-ventral equator region [56]. In contrast, the spatially defined overexpression or knockdown of *pnr* using a *pnr*-Gal4 driver (this work) may highlight later functions of Pnr in regulating the eye *vs.* head ratio. Interestingly, in line with our results, cuticle overgrowth has been observed for some *ey*-Gal4 induced loss of function clones [56]. Overall, our results and previous reports highlight the importance to analyse gene functions in temporally and spatially well-defined experiments to disentangle the context-dependent role of pleiotropic developmental regulators such as Pnr.

Besides the temporal and spatial control of gene expression, the function of transcription factors can be further diversified by the presence of co-factors. Our combinatorial RNAseq and ATACseq data revealed more than 1,000 putative Pnr target genes expressed during eye-antennal disc development, of which some genes showed expression profiles in agreement with the reported activating role of Pnr, while some targets showed signatures of a negative relationship. It has been shown that Pnr plays a dual regulatory role in the wing disc [84,85] where its repressive function is realized upon heterodimerization with its co-factor Ush [57,60]. Although it was previously reported that *ush* was not expressed or non-functional [50] in the developing eye-antennal disc, we show here for the first time that *ush* is transcribed in this tissue and that the Ush protein is co-localized with Pnr in the squamous cells of the dorsal peripodial epithelium and in the cuboidal cells of the disc margin. Furthermore, *ush* expression is necessary for proper head development, since knock down in the dorsal part of the eye-antennal disc resulted in irregularities in adult dorsal head cuticle and the head bristle pattern (this work and see [63] for bristle phenotype). The co-expression of *pnr* and *ush* as well as their involvement in the development of the same morphological structures strongly suggest that

they interact during eye-antennal disc development. Accordingly, we showed that Pnr is involved in *ush* activation. Although we cannot rule out an indirect interaction because we did not find *ush* as a potential target gene of Pnr, our findings are in line with the interaction of these two factors in the developing wing disc [85]. Furthermore, the overexpression of Ush resulted in a slight repression of Pnr as well as a double antenna phenotype reminiscent of that observed upon loss of Pnr function [50,61]. This data in combination with our finding that *pnr* itself is a putative Pnr target gene implies that the expression level of *pnr* might be kept in balance via activation by Pnr alone and repression by the Pnr-Ush heterodimer. This model suggests that the stoichiometry between Pnr and its co-factor Ush is crucial for proper eye-antennal disc development.

Support for this hypothesis comes from the bristle phenotypes in our gain- and loss of function experiments. In the wing disc Pnr and Ush control the positioning of proneural cell clusters, which give rise to sensory bristles on the thorax, by regulating the proneural genes *achaete* (*ac*) and *scute* (*sc*) [63,86,87]. Thoracic sensory bristles develop in regions with high *pnr* and low *ush* expression [60,63]. Accordingly, Pnr overexpression in the eye-antennal disc consistently resulted in duplication of the anterior vertical bristles in the adult head. Most probably, these extra bristles arise where *pnr* overexpression cannot be compensated by Ush. This is reminiscent of the phenotype of a dominant pnr^{D} allele [86] that is characterized by a loss of its ability to dimerize with Ush [86,88]. Overexpression of *ush* in most of the dorsal peripodial epithelium resulted not only in loss of the posterior vertical bristles, but also in loss of the anterior vertical bristles, suggesting that extra Ush above a certain threshold completely antagonizes Pnr function and subsequent sensory bristle formation. While we observed bristle phenotypes in our functional assays, the stereotypic bristle pattern in the dorsal head is conserved between *D. melanogaster* and *D. mauritiana* even though *pnr* and *ush* were differentially expressed in our dataset. Interestingly, both genes showed higher expression in *D. mauritiana* at 72 and 96 h AEL with a similar ratio of both factors (Supplementary Figure 11). In contrast, a different ratio was observed at 120 h AEL, with *pnr* expression being higher in *D. mauritiana*, while *ush* expression was more similar in both species at this later stage (Supplementary Figure 11). Together with the fact that most of these proneural cell clusters are already specified 18h to 6h prior to puparium formation [89], this suggests that especially at these earlier stages (72h – 96h AEL), the ratio between the two co-factors must remain stable to ensure proper sensory bristle formation. However, once bristle formation is defined,

variation in the ratio of both factors at later stages can cause natural variation in dorsal head cuticle shape in the occipital region and dorsal head development without affecting bristle formation.

Taken together, we identified variation in expression of a highly pleiotropic regulatory module composed of Pnr and Ush that causes the differential expression of a plethora of potential target genes. Since the observed expression differences are associated with phenotypic variation, we conclude that this regulatory module represents a tuning node in the GRN underlying head and eye development in *Drosophila*. Interestingly, Pnr is not the only central and pleiotropic factor implicated in natural variation in head shape and eye size. It has recently been shown that a single point mutation in the *cis*-regulatory sequence of *ey*, one of the most upstream factors of the retinal determination network [38], leads to heterochronic changes in its regulation and subsequent variation in eye size among *D. melanogaster* laboratory strains. Quantitative genetics data for other evolving morphological traits, such as pelvic reduction in stickleback [7] and variation in *Drosophila* trichome patterns [6] also identified genetic variants associated with central pleiotropic developmental factors. Hence, morphological evolution seems to be predominantly driven by natural variation in expression of highly connected pleiotropic tuning nodes. Systematic analyses of GRN connectivity confirmed that developmental regulators tend to be highly connected [90,91]. While a high level of connectivity ensures the buffering of expression fluctuations, the opposite effect has been observed as well. Data obtained in yeast showed that genes that are regulated by many other factors (*trans*-mutational target size) and genes that contain many transcription factor binding motifs (*cis*-mutational target size) are more prone to accumulate mutations. In turn, these can affect gene expression [13,92] allowing for their incorporation in many different GRNs. Consequently, a complex gene regulation facilitates the remodeling of regulatory interactions in a temporally and spatially specific manner.

Eye-antennal disc development is highly complex and the regulatory interactions within the underlying GRN are variable both throughout time [41] and in different parts of the disc [93], facilitating the use of the same developmental gene products in different contexts. For instance, genes of the retinal determination network are required for the initial proliferation and growth of the entire eye-antennal disc [44,94,95] and later they play a pivotal role in retinal specification [38,40]. These distinct roles have been suggested to be achieved by considerable

rewiring of the respective GRNs, which allows them to fulfil temporally and even spatially restricted tasks [96]. The various described roles for Pnr [50,56], its continuous expression in the dorsal eye-antennal disc and the observation that variation in *pnr* expression affects overall head shape and eye size simultaneously, strongly suggest that Pnr as well is involved in several sub-networks during eye and head development. The interaction with co-factors, such as Ush provides a mechanism of modulating the role of Pnr from an activating to a repressing transcription factor and its usage in spatially defined GRNs. We propose that the dynamic nature of GRNs is facilitated by complex gene regulation and may explain how interspecific variation in expression of a highly pleiotropic and central transcription factor such as Pnr can result in remodelling of the transcriptomic landscape in an otherwise tightly controlled network.

Since the trade-off between eye size and head cuticle seems to be a common feature of *Drosophila* [30,31,34,35,75–77], this trait represents an excellent model to test whether natural variation in different lineages results from changes in the same nodes of the underlying GRN or not. Between *D. melanogaster* and *D. simulans* different QTL regions were identified for eye size and the width of the interstitial cuticle. This observation was supported by quantitative developmental data showing that the anlagen for the head cuticle start to diverge in size prior to the retinal tissue [30]. Therefore, the trade-off seems to be regulated by independent factors in these two species. However, recent quantitative genetics analyses identified some loci that affect eye size and head cuticle in opposite directions in intraspecific comparisons in *D. melanogaster* and *D. simulans* [31,32]. Additionally, our finding that variation in *pnr* expression influences both traits simultaneously further suggests that they may be genetically linked in *D. melanogaster* and *D. mauritiana*. Therefore, a convergent evolution of the trade-off in *Drosophila* is likely. A detailed analysis of the morphological basis of eye size differences showed that bigger eyes can be the result of differences in ommatidia number (e.g. between *D. melanogaster* and *D. mauritiana*, this work and [34]) or ommatidia size (e.g. between *D. simulans* and *D. mauritiana*, [30,34]). Since these two features are regulated at different time-points and developmental processes, it is conceivable that the molecular and developmental basis of eye size differences varies in different groups. In summary, our current knowledge based on quantitative genetics, developmental as well as morphological data suggests that different nodes within the GRN underlying head and eye development may evolve to give rise to variation in head morphology in *Drosophila*.

We provide here a framework to reveal tuning nodes within GRNs and to subsequently validate these findings. Our comparative transcriptomics approach can be used as entry point to study the evolution of complex morphological traits or it can be applied to link already identified genetic variation to nodes within developmental GRNs and to developmental processes. It is important to note, however, that this approach unfolds its full potential if complemented with quantitative genetics data that allows identifying exact genetic variants associated with trait variation. The fact that we were able to shift *D. melanogaster* head shapes only to a certain degree towards a *D. mauritiana* head shape suggests that multiple genomic loci are responsible for the observed morphological divergence between *D. melanogaster* and *D. mauritiana*. Furthermore, it remains to be established whether the *pnr* and/or *ush* loci contain genetic variants associated with eye size and head shape differences. Quantitative genetics approaches are not applicable since interspecific crosses between *D. melanogaster* and *D. mauritiana* result in infertile F1 females [97]. However, reciprocal hemizygosity tests [98] for Pnr, Ush and putative regulators of these two factors represent a powerful tool to further dissect the causative genetic variants in the future. Overall, much more genetic as well as developmental data from different groups are necessary to draw a full picture of this exciting morphological phenomenon.

Material and Methods

Generation of the transcriptomic dataset

Flies from the following strains were raised at 25°C at a 12:12 dark:light cycle for at least two generations and their eggs were collected on agar plates for one hour: *D. melanogaster* (OreR), *D. mauritiana* (TAM16). 30 L1 larva were collected in vials and developing eye-antennal discs were dissected at 72h AEL (120–130 discs; male and female), 96h AEL (80–90 discs; female) and 120h AEL (40-50 discs; female) and stored in RNALater (Quiage, Venlo, Netherlands). For each species and stage 3 biological replicates were dissected. Total RNA was isolated using the Trizol (Invitrogen, Thermo Fisher Scientific, Waltham, Massachusetts, USA) method according to the manufacturer's recommendations and the samples were DNAseI (Sigma, St. Louis, Missouri, USA) treated in order to remove DNA contamination. RNA quality was determined using the Agilent 2100 Bioanalyzer (Agilent Technologies, Santa Clara, CA, USA) microfluidic electrophoresis. Only samples with comparable RNA integrity were selected for sequencing. Library preparation for RNA-seq was performed using the TruSeq RNA Sample

Preparation Kit (Illumina, catalog ID RS-122-2002) starting from 500 ng of total RNA. Accurate quantitation of cDNA libraries was performed using the QuantiFluordsDNA System (Promega, Madison, Wisconsin, USA). The size range of final cDNA libraries was determined applying the DNA 1000 chip on the Bioanalyzer 2100 from Agilent (280 bp). cDNA libraries were amplified and sequenced (50 bp single-end reads) using cBot and HiSeq 2000 (Illumina). Sequence images were transformed to bcl files using the software BaseCaller (Illumina). The bcl files were demultiplexed to fastq files with CASAVA (version 1.8.2)

Mapping

The reads were mapped against strain-specific transcriptomes (*D. melanogaster* and *D. mauritiana*), including CDS and UTR [99] using Bowtie2 v. 2.3.4.1 [100] with the following parameters: `-very-sensitive-local -N1`. Samtools version 1.9 [101,102] was used to further process the reads and count the reads mapped to each transcript (idxstats).

Differential expression analysis and data visualization

The PCA plot is based on the regularized log (rlog) transformation from the DESeq2 package (DESeq2_1.22.2 [103]; R version 3.5.2).

DeSeq2 was used to perform a pairwise differential expression analysis between the two species at each time point using the `apeglm` option as shrinkage estimator [104] (*D. melanogaster* 72h vs. *D. mauritiana* 72h, *D. melanogaster* 96h vs. *D. mauritiana* 96h and *D. melanogaster* 120h vs. *D. mauritiana* 120h). We used the online tool Metascape [105] to perform GO enrichment analysis for each time point. We combined the read counts of all genes that were significantly differentially expressed (log2FC > 0 | log2FC < 0 and padj < 0.05) between the two species in at least one stage (8,350 genes in total). We then clustered them according to their expression dynamics (i.e. we treated the combined data from both species as a time-series) using the coseq package (version 1.6.1) [106,107] with the following parameters: `K=2:25, transformation="arcsin", norm="TMM", model="Normal"`. We searched for potential upstream factors 5 kb upstream of the transcription start site, 5'UTR regions and 1st introns using the i-cisTarget tool [108,109] keeping the default parameters: Minimum fraction of overlap: 0.4, NES: 3.0, ROC threshold for AUC calculation: 0.01. Supplementary Table S2 contains enriched unique motifs with NES > 4.0, we excluded non-*Drosophila* motifs, and added only the ones which could be found on Flybase [110]. To check which of these potential upstream

regulators are differentially expressed, we removed all duplicates and overlapped the list with all significantly differentially expressed genes.

Metascape was used to analyse differential enrichment of GO terms for each pairwise comparison.

Generation of the ATACseq dataset

For the generation of ATAC-seq datasets we followed a previously established protocol [111]. Developing eye-antennal discs of *D. melanogaster* were dissected in ice-cold PBS at 72h, 96h and 120h AEL. PBS was removed and exchanged for 50 µl lysis buffer (10 mM Tris-HCl (pH = 7.4); 10 mM NaCl; 3 mM MgCl2; 0.1 % IGEPAL). The mixture was pipetted several times up and down to lyse the cells and then split into micro centrifuge tubes. Centrifugation for 10 min at 500 g and 4°C. The cell number was assessed in one of the samples and between 50,000 and 80,000 nuclei were used in subsequent steps. The supernatant was removed, and the pellet(s) were dissolved in 47.5 µl 1X tagmentation buffer (20 mM Tris-CH3COOH (pH = 7.6); 10 mM MgCl2; 20 % (vol/vol) dimethylformamide) with 2.5 µl Tn5 Transposase and then incubated for 30 min at 37°C. For purification we used the QIAGEN MinElute Kit and eluted in 10 µl Elution Buffer (10 mM Tris, pH = 8). The PCR amplification was done as follows: 10 µl tagmented chromatin, 10 µl H2O, 2.5 µl Nextera PCR primer 1*, 2.5 µl Nextera PCR primer 2**, 25 µl NEBNext High-Fidelity 2X PCR Master Mix (Cat #M0541).

* AATGATACGGCGACCACCGAGATCTACACTCGTCGGCAGCGTCAGATGTG

**	Ad2.2_CGTACTAG	CAAGCAGAAGACGGCATACGAGATCTAGTACGGTCTCGTGGGCTCGGAGATGT
	Ad2.3_AGGCAGAA	CAAGCAGAAGACGGCATACGAGATTTCTGCCTGTCTCGTGGGCTCGGAGATGT
	Ad2.4_TCCTGAGC	CAAGCAGAAGACGGCATACGAGATGCTCAGGAGTCTCGTGGGCTCGGAGATGT
	Ad2.5_GGACTCCT	CAAGCAGAAGACGGCATACGAGATAGGAGTCCGTCTCGTGGGCTCGGAGATGT
	Ad2.6_TAGGCATG	CAAGCAGAAGACGGCATACGAGATCATGCCTAGTCTCGTGGGCTCGGAGATGT
	Ad2.7_CTCTCTAC	CAAGCAGAAGACGGCATACGAGATGTAGAGAGGTCTCGTGGGCTCGGAGATGT

We used the following program: 1) 72 °C for 5 min, 2) 98 °C for 30 sec, 3) 98 °C for 10 sec, 4) 63 °C at 30 sec, 5) 72 °C for 1 min, step 3) -5) were repeated 13 times. This was followed by another 2x purification step with the QIAGEN MinElute Kit: elution in 2 X 10 µl Elution Buffer (10 mM Tris, pH = 8).

Bioinformatic processing of the ATACseq data

We performed quality checks of the sequenced reads using FASTQC (https://www.bioinformatics.babraham.ac.uk/projects/fastqc/). The reads were trimmed using

Trimmomatic (version 0.36) [112] with the parameters `slidingwindow 4:15` and `minlen 30`. Trimmed reads were mapped to the *D. melanogaster* genome (version 6.13) (after discarding the mitochondrial genome) using Bowtie2 (version 2.3.4.3), with the commands: `--no-unal` and `-X2000`. Samtools version 1.9 was subsequently used to convert the sam files to bam files, and to sort and index bam files. We removed duplicates using PICARD (version 2.1.1., http://broadinstitute.github.io/picard/) with default parameters and converted the resulted bam files to bed files. Reads were then centred as described in [111]. We used MACS2 (version 2.1.2) [113] with the following commands: `-g dm --nomodel --shift -100 --extsize 200 -q 0.01 -bdg` to call significant peaks. We used the Integrated Genome Browser (IGB) [114] to visualize the read depth and peaks. Peaks were annotated to the closest gene using the `annotatePeaks.pl` program from the HOMER software package (v4.8.3) [115] using `dm6` as genomic input.

Definition of a Pnr target gene list

As a basis for the high confidence list of putative Pnr target genes a Chip-chip dataset was used (downloaded on 1st of July, 2015 from http://furlonglab.embl.de/data/download), which comprises ChIP-chip experiments in the *Drosophila* embryo with several transcription factors, including Pnr at two time points (4-6h AEL and 6-8h AEL) [116]. All Pnr-binding regions from both time points were selected with a Tile-Map score of <5.5. and where the distance of the centre of the peak to the transcription start site was -1000 bp and +1000 bp. We performed a *de novo* motif search in these peak regions, to define the Pnr binding motif. We used this motif to screen a set of combined and unique ATAC-seq peaks from three time-points for potential Pnr binding sites in open chromatin regions of the developing eye-antennal disc, which resulted in 1,335 unique peaks in total. These peaks were annotated to 1,241 genes, of which 1,060 (Supplementary Table 3) are expressed in the eye antennal disc (>= 10 reads in at least one of the three stages). We overlapped these genes with all genes that were significantly differentially expressed in at least one of the three stages (8,350 genes). To understand the expression dynamics of potential Pnr target genes in relation to Pnr itself, we performed hierarchical clustering according to their expression dynamics using coseq with the following parameters: `K=2:25, transformation="arcsin", norm="TMM", model="kmeans"`.

We downloaded all known direct (TF-gene, 157,462 interactions) or genetic interactions (14,241 interactions) from the DroID database [58,59] (in total 171,703 interactions). We extracted from this database all interactions of Pnr with other genes and found 181 target genes of Pnr. 26 of these were present our Pnr target gene list and 17 were differentially expressed. We used Cytoscape [117] to visualize the interaction between these target genes and potential upstream regulators found in the database.

Antibody generation and immunohistology

We generated polyclonal antibodies against Pnr [116] and Ush [61] based on previous knowledge against the following peptide sequences (Proteintech, Rosemont, IL, USA):

Pnr_B (125-294):
TPLWRRDGTGHYLCNACGLYHKMNGMNRPLIKPSKRLVSATATRRMGLCCTNCGTRTTTLWRRNNDGE
PVCNACGLYYKLHGVNRPLAMRKDGIQTRKRKPKKTGSGSAVGAGTGSGTGSTLEAIKECKEEHDLKPSLSL
ERHSLSKLHTDMKSGTSSSSTLMGHHSAQQ

Pnr_B (206-336):

GVNRPLAMRKDGIQTRKRKPKKTGSGSAVGAGTGSGTGSTLEAIKECKEEHDLKPSLSLERHSLSKLHTDM
KSGTSSSSTLMGHHSAQQQQQQQQQQQQQQQQQQQQQSAHQQCFPLYGQTTTQQQHQQHGH

Ush (231-250):

CSHRIKDTDEAGSDKSGAGG

Ush (1174-1191):

VGGHGQQKNKENLQEAAI

Before usage, both antibodies were preabsorbed overnight in a mix of *Drosophila* embryos on 4°C.

Developing eye-antennal discs were dissected and fixed for 30 min in 4% paraformaldehyde (PFA). For this purpose, PFA was dissolved in ddH_2O and 1M NaOH by boiling, diluted with 10x Phosphate Buffered Saline (PFA) and the pH was adjusted to 7.2 using NaOH. The discs were then washed 3 times in 0.03% PBT (1x PBS, 0.03% Triton X-100) before blocking in 5% normal goat serum for 30 min. Incubation with the primary antibody was done for 90 min, before 3 additional washing steps with PBT and one round of blocking for 30 min. The discs were then incubated with the secondary antibody overnight on a rocking plate at 4°C. Phalloidin-488 (1:100) was added. After 3 washing steps with PBT, the discs were incubated

with DAPI (1:1000) for 10 min, followed by one washing step with PBT and one washing step with PBS. Subsequently, the discs were mounted in mounting medium (80% glycerol + 4% n-propyl-galate) and kept at least one night on 4°C prior to imaging.

We confirmed the specificity of the Ush antibody by recapitulating known Ush expression domains in the wing imaginal disc (Supplementary Figure 12a) and during embryonic development (Supplementary Figure 12b,c). For test stainings in embryos we collected embryos for several hours on apple agar plates, removed the chorion with 50% bleach (DanKlorix) and rinsed them 3 times with 0.03% PBT (Phosphate buffered saline 1%, Triton X-100). We fixed the embryos with heptane and 2% formaldehyde for 20min and washed with MeOH, followed by washing steps with PBT. The embryos were then blocked in 3% BSA for one hour, followed by incubation with the primary antibody overnight. After two washing steps with PBT, we added HRP-coupled secondary antibody for 90 min. After three washing steps with PBT we performed a DAB (3'-3diaminobenzidine) staining. The embryos were then washed again 2 times in PBT and mounted in glycerol.

Concentrations antibodies used: Anti-Pnr (rabbit): 1:200 (Proteintech, Rosemont, IL, USA), Anti-Ush (rabbit): 1:2000 (Proteintech, Rosemont, IL, USA), Anti-GFP (chicken): 1:1000 (Abcam # 13970, kindly provided by Dr. Marita Büscher); Concentrations Secondary antibodies: Anti-Chicken-488 (Invitrogen Cat# A-11039, kindly provided by Dr. Marita Büscher); Anti-Rabbit-Cy3 (donkey): 1:500 (Jackson ImmunoResearch #711-165-152, kindly provided by Kolja N. Eckermann); Anti-rabbit-HRP-coupled (1:1000) (Jackson ImmunoResearch #111-035-003, kindly provided by Dr. Marita Büscher).

Pictures of eye-antennal discs upon antibody staining were taken using a Zeiss LSM 710 confocal microscope. Antibody stainings were visualized and processed with Fiji software. Vertical sections of the confocal pictures were generated using the Volume Viewer plugin using the following parameters: Display Mode: Slice and Boarders, Interpolation: Nearest Neighbour, Transfer Function: Fire LUT.

Geometric Morphometrics

We imaged dorsal heads of wildtype specimens from each parental line, as well as the offspring of the respective *D. melanogaster* crosses using a Leica M205 FA stereo microscope. We placed 64 landmarks on pictures of these dorsal heads using the tpsDig2 software [118]. We then defined 23 fixed landmarks and 41 sliding landmarks using tpsUtil [118]. tpsRelw32 [118] was

used to calculate the consensus (i.e. Procrustes superimposition), partial warps and relative warps. Using MorphoJ [119] for visualization, we performed Procrustes Fit and generated a covariance matrix. To analyse differences in dorsal head shapes in wildtype *D. melanogaster* and *D. mauritiana*, we performed canonical variate analysis (CVA) using MorphoJ. We further performed a principal component analysis (PCA) to analyse difference in head shapes upon knock-down or up-regulation of *pnr*.

Overexpression/Knock-down of *pnr* and *ush*

To overexpress or knock-down *pnr* and *ush*, the following fly lines were used:

D. melanogaster (Oregon R) and *D. mauritiana* (TAM 16) (both kindly provided by Alistair McGregor, Oxford Brookes University), *pnr* GAL4/TM6B (kindly provided by Marc Haenlin), *pnr*-GAL4>UAS2YFP/TM6B (kindly provided by Marc Haenlin, CBI Toulouse), *ush*-GAL4 26662 (y[1] w[*]; P{w[+mW.hs]=GawB}*ush*[MD751]), Bloomington; UAS-*ush*14IIA/CyO (kindly provided by Marc Haenlin, CBI Toulouse); *ush*-RNAi 3622 (y[1] v[1]; P{y[+t7.7] v[+t1.8]=TRiP.HM05193}attP2/TM3, Sb[1]), Bloomington; UAS-*pnr* (w; UAS-*pnr*/CyO; TM2/TM6B) (kindly provided by Fernando Casares); *pnr*-RNAi (VT101522/KK, #108962 VDRC Stock Center and VT6224/GD, #1511 VDRC Stock Center); *oc*-Gal4/CyO (kindly provided by Fernando Casares); UAS-Stinger-GFP (nGFP) (kindly provided by Dr. Gerd Vorbrüggen).

All crosses were performed at 25°C and at a constant 12h:12h light:dark cycle. Since Pnr and Ush are crucial during embryonic development, we chose combinations of GAL4/UAS lines that resulted in a phenotype, but were not lethal during embryonic, larval or pupal stages. We used a set of GAL4 lines representing a range from weak to strong drivers and in the case of *pnr*-RNAi we used two independent RNAi lines.

Pnr expression and lineage tracing

The *pnr-GAL4* line *pnrMD237* [120], recombined with UAS-GFP, was used to follow *pnr* expression in imaginal and pupal eye-antennal discs. The adult *pnr* expression domain in adult heads was monitored in *y; pnr-GAL4/UAS-y+* flies [120] as the cuticle region with y-rescued pigmentation. To follow the *pnr-GAL4* lineage, *pnr-GA4*, UAS-GFP flies were crossed to UAS-flipase; *act5c>stop< nuc-lacZ* flies [121]. In the discs of the progeny, actual *pnr* expression was visualized with anti-GFP and its lineage with anti β-galactosidase.

Immunostaining and imaging.

Third instar or pupal discs were processed as in [83]. Primary antibodies were chicken anti-GFP (1:500; ab13970, Abcam), rabbit anti-β-galactosidase (1:1000; Cappel) and mouse anti-Eya (1:500; 10H6, Developmental Studies Hybridoma Bank, Iowa University). Secondary antibodies at 1:400 were from Molecular Probes. Imaging was carried out on a Leica SPE confocal setup (ALMI, CABD).

Adult head cuticle preparation.

Dissected adult heads in PBS were mounted in Hoyer's medium: Lactic Acid (50:50) as in [83].

Ommatidia Counting

To estimate ommatidia number of single fly eyes, we took pictures of one eye per fly (50 stacks/eye) using a Leica M205 FA stereo microscope and an external light source, which resulted in reflection of light by each ommatidium. We used FIJI to perform Z-projections using maximum intensity and then transformed each picture to make sure that the single reflection of each ommatidium is represented by a black dot (i.e. increase of contrast, transform to grey scale and invert photo). We then used the ITCN cell counter tool (with the following parameters: Width: 7, Minimum Distance: 17, Threshold: 1.5; https://bioimage.ucsb.edu/search/node/itcn) to estimate the number of black dots, i.e. the number ommatidia. Statistical analysis of ommatidia number was done using a one-way ANOVA and pair-wise comparisons were calculated using Tukey HSD test.

Funding

NP and EB are funded by the Deutsche Forschungsgesellschaft (DFG, Grant Number: PO 1648/3-1) to NP. FC acknowledges funding through grants BFU2015-66040-P, PGC2018-093704-B-I00 and MDM-2016-0687, from Ministerio de Ciencia, Innovación y Universidades of Spain.

Author contribution

EB: Conceptualization, Data curation, Formal analysis, Investigation, Methodology, Visualization, Writing – original draft, Writing- review and editing. AB: Investigation. SA: Investigation. DS: Investigation. CMH: Investigation. AN: Investigation. IA: Resources, Writing – review and editing, MTO: Investigation, Resources, Writing – review and editing, FC: Investigation, Writing- review and editing. NP: Conceptualization, Funding acquisition, Project administration, Resources, Supervision, Visualization, Writing – original draft, Writing – review and editing.

Acknowledgments

Many thanks to Marita Büscher and Kolja Eckermann for sharing antibodies and to Alistair P. McGregor, Marc Haenlin and Gerd Vorbrüggen for sharing *Drosophila* stocks. We are grateful for financial support for the ATACseq data to Alistair P. McGregor. Stocks obtained from the Bloomington Drosophila Stock Center (NIH P40OD018537) were used in this study. Many thanks to the Deep-Sequencing Core Facility of the Universitätsmedizin Göttingen (UMG) for next generation sequencing. We are grateful for many fruitful discussions and feedback from members of the Department of Developmental Biology and Posnien Lab members.

References

1. Alberch, P. From genes to phenotype: dynamical systems and evolvability. *Genetica* **84,** 5–11; 10.1007/bf00123979 (1991).
2. Lewontin, R. C. *The genetic basis of evolutionary change* (Columbia Univ. Pr, New York, 1974).
3. Rebeiz, M., POOL, J. E., Kassner, V. a., AQUADRO, C. F. & Carroll, S. B. Stepwise modification of a modular enhancer underlies adaptation in a Drosophila population. *Science* **326,** 1663–1667; 10.1126/science.1178357 (2009).
4. Jeong, S., Rokas, A. & Carroll, S. B. Regulation of body pigmentation by the Abdominal-B Hox protein and its gain and loss in Drosophila evolution. *Cell* **125,** 1387–1399; 10.1016/j.cell.2006.04.043 (2006).
5. Hoekstra, H. E., Hirschmann, R. J., Bundey, R. A., Insel, P. A. & Crossland, J. P. A single amino acid mutation contributes to adaptive beach mouse color pattern. *Science* **313,** 101–104; 10.1126/science.1126121 (2006).
6. McGregor, A. P. *et al.* Morphological evolution through multiple cis-regulatory mutations at a single gene. *Nature* **448,** 587–590; 10.1038/nature05988 (2007).
7. Shapiro, M. D. *et al.* Genetic and developmental basis of evolutionary pelvic reduction in threespine sticklebacks. *Nature* **428,** 717–723; 10.1038/nature02415 (2004).
8. Menuet, A., Alunni, A., Joly, J.-S., Jeffery, W. R. & Rétaux, S. Expanded expression of Sonic Hedgehog in Astyanax cavefish. Multiple consequences on forebrain development and evolution. *Development* **134,** 845–855; 10.1242/dev.02780 (2007).
9. Stemmer, M., Schuhmacher, L.-N., Foulkes, N. S., Bertolucci, C. & Wittbrodt, J. Cavefish eye loss in response to an early block in retinal differentiation progression. *Development* **142,** 743–752; 10.1242/dev.114629 (2015).
10. Davidson, E. H. Emerging properties of animal gene regulatory networks. *Nature* **468,** 911–920; 10.1038/nature09645 (2010).
11. Kitano, H. Biological robustness. *Nature Reviews Genetics* **5,** 826–837; 10.1007/978-3-7643-7567-6_10 (2004).
12. Waddington, C. H. CANALIZATION OF DEVELOPMENT AND THE INHERITANCE OF ACQUIRED CHARACTERS. *Nature* **150,** 563–565; 10.1038/150563a0 (1942).
13. Landry, C. R., Lemos, B., Rifkin, S. a., Dickinson, W. J. & Hartl, D. L. Genetic properties influencing the evolvability of gene expression. *Science* **317,** 118–121; 10.1126/science.1140247 (2007).

14. Batada, N. N. & Hurst, L. D. Evolution of chromosome organization driven by selection for reduced gene expression noise. *Nat Genet* **39,** 945–949; 10.1038/ng2071 (2007).

15. Lehner, B. Selection to minimise noise in living systems and its implications for the evolution of gene expression. *Molecular systems biology* **4,** 170; 10.1038/msb.2008.11 (2008).

16. Giaever, G. *et al.* Functional profiling of the Saccharomyces cerevisiae genome. *Nature* **418,** 387–391; 10.1038/nature00935 (2002).

17. Kamath, R. S. *et al.* Systematic functional analysis of the Caenorhabditis elegans genome using RNAi. *Nature* **421,** 231–237; 10.1038/nature01278 (2003).

18. Costanzo, M. *et al.* The genetic landscape of a cell. *Science (New York, N.Y.)* **327,** 425–431; 10.1126/science.1180823 (2010).

19. Tsai, A., Alves, M. R. & Crocker, J. Multi-enhancer transcriptional hubs confer phenotypic robustness. *eLife* **8**; 10.7554/eLife.45325 (2019).

20. Frankel, N. *et al.* Phenotypic robustness conferred by apparently redundant transcriptional enhancers. *Nature* **466,** 490–493; 10.1038/nature09158 (2010).

21. Gavin-Smyth, J., Wang, Y. C., Butler, I. & Ferguson, E. L. A genetic network conferring canalization to a bistable patterning system in Drosophila. *Current Biology* **23,** 2296–2302; 10.1016/j.cub.2013.09.055 (2013).

22. Hollenhorst, P. C., Shah, A. A., Hopkins, C. & Graves, B. J. Genome-wide analyses reveal properties of redundant and specific promoter occupancy within the ETS gene family. *Genes & Development* **21,** 1882–1894; 10.1101/gad.1561707 (2007).

23. Mackay, T. F. C., Stone, E. a. & Ayroles, J. F. The genetics of quantitative traits. Challenges and prospects. *Nature Reviews Genetics* **10,** 565–577; 10.1038/nrg2612 (2009).

24. Mackay, T. F. Quantitative trait loci in Drosophila. *Nature Reviews Genetics* **2,** 11–20; 10.1038/35047544 (2001).

25. Boyle, E. A., Li, Y. I. & Pritchard, J. K. An Expanded View of Complex Traits: From Polygenic to Omnigenic. *Cell* **169,** 1177–1186; 10.1016/j.cell.2017.05.038 (2017).

26. Pallares, L. F. *et al.* Mapping of Craniofacial Traits in Outbred Mice Identifies Major Developmental Genes Involved in Shape Determination. *PLoS Genetics* **11,** e1005607; 10.1371/journal.pgen.1005607 (2015).

27. Burgio, G., Baylac, M., Heyer, E. & Montagutelli, X. Genetic analysis of skull shape variation and morphological integration in the mouse using interspecific recombinant congenic strains between C57BL/6 and mice of the mus spretus species. *Evolution* **63,** 2668–2686; 10.1111/j.1558-5646.2009.00737.x (2009).

28. Maga, A. M., Navarro, N., Cunningham, M. L. & Cox, T. C. Quantitative trait loci affecting the 3D skull shape and size in mouse and prioritization of candidate genes in-silico. *Frontiers in physiology* **6,** 92; 10.3389/fphys.2015.00092 (2015).

29. Pallares, L. F., Harr, B., Turner, L. M. & Tautz, D. Use of a natural hybrid zone for genomewide association mapping of craniofacial traits in the house mouse. *Molecular Ecology* **23,** 5756–5770; 10.1111/mec.12968 (2014).

30. Arif, S. *et al.* Genetic and developmental analysis of differences in eye and face morphology between Drosophila simulans and Drosophila mauritiana. *Evolution & Development* **15,** 257–267; 10.1111/ede.12027 (2013).

31. Norry, F. M. & Gomez, F. H. Quantitative Trait Loci and Antagonistic Associations for Two Developmentally Related Traits in the Drosophila Head. *Journal of Insect Science* **17,** 19; 10.1093/jisesa/iew115 (2017).

32. Gaspar, P. *et al.* Characterization of the Genetic Architecture Underlying Eye Size Variation Within Drosophila melanogaster and Drosophila simulans. *G3 (Bethesda, Md.)*; 10.1534/g3.119.400877 (2020).

33. Arda, H. E. & Walhout, A. J. M. Gene-centered regulatory networks. *Briefings in Functional Genomics* **9,** 4–12; 10.1093/bfgp/elp049 (2010).

34. Posnien, N. *et al.* Evolution of eye morphology and rhodopsin expression in the Drosophila melanogaster species subgroup. *PLoS ONE* **7,** e37346; 10.1371/journal.pone.0037346 (2012).

35. Hilbrant, M. *et al.* Sexual dimorphism and natural variation within and among species in the Drosophila retinal mosaic. *BMC evolutionary biology* **14,** 240; 10.1186/s12862-014-0240-x (2014).

36. Haynie, J. L. & Bryant, P. J. Development of the eye-antenna imaginal disc and morphogenesis of the adult head in Drosophila melanogaster. *The Journal of experimental zoology* **237,** 293–308; 10.1002/jez.1402370302 (1986).

37. Amore, G. & Casares, F. Size matters. The contribution of cell proliferation to the progression of the specification Drosophila eye gene regulatory network. *Developmental Biology* **344,** 569–577; 10.1016/j.ydbio.2010.06.015 (2010).

38. Casares, F. & Almudi, I. in *Organogenetic Gene Networks,* edited by J. Castelli-Gair Hombría & P. Bovolenta (Springer International Publishing, Cham, s.l., 2016), pp. 95–124.

39. Kumar, J. P. The molecular circuitry governing retinal determination. *Biochimica et Biophysica Acta - Gene Regulatory Mechanisms* **1789,** 306–314; 10.1016/j.bbagrm.2008.10.001 (2009).

40. Treisman, J. E. Retinal differentiation in Drosophila. *Wiley Interdisciplinary Reviews: Developmental Biology* **2,** 545–557; 10.1002/wdev.100 (2013).

41. Torres-Oliva, M., Schneider, J., Wiegleb, G., Kaufholz, F. & Posnien, N. Dynamic genome wide expression profiling of Drosophila head development reveals a novel role of Hunchback in retinal glia cell development and blood-brain barrier integrity. *PLoS Genetics* **14,** e1007180; 10.1371/journal.pgen.1007180 (2018).

42. Mishra, A. K., Bargmann, B. O. R., Tsachaki, M., Fritsch, C. & Sprecher, S. G. Functional genomics identifies regulators of the phototransduction machinery in the Drosophila larval eye and adult ocelli. *Developmental Biology* **410,** 164–177; 10.1016/j.ydbio.2015.12.026 (2016).

43. Zheng, L. & Carthew, R. W. Lola regulates cell fate by antagonizing Notch induction in the Drosophila eye. *Mechanisms of Development* **125,** 18–29; 10.1016/j.mod.2007.10.007 (2008).

44. Neto, M. *et al.* Nuclear receptors connect progenitor transcription factors to cell cycle control. *Scientific Reports* **7,** 4845; 10.1038/s41598-017-04936-7 (2017).

45. Brennan, C. A., Ashburner, M. & Moses, K. Ecdysone pathway is required for furrow progression in the developing Drosophila eye. *Development* **125,** 2653–2664 (1998).

46. Sekelsky, J. J., Newfeld, S. J., Raftery, L. A., Chartoff, E. H. & Gelbart, W. M. Genetic characterization and cloning of mothers against dpp, a gene required for decapentaplegic function in Drosophila melanogaster. *Genetics* **139,** 1347–1358 (1995).

47. Cordero, J. B., Larson, D. E., Craig, C. R., Hays, R. & Cagan, R. Dynamic decapentaplegic signaling regulates patterning and adhesion in the Drosophila pupal retina. *Development* **134,** 1861–1871; 10.1242/dev.002972 (2007).

48. Wiersdorff, V., Lecuit, T., Cohen, S. M. & Mlodzik, M. Mad acts downstream of Dpp receptors, revealing a differential requirement for dpp signaling in initiation and propagation of morphogenesis in the Drosophila eye. *Development* **122,** 2153–2162 (1996).

49. Wells, B. S., Pistillo, D., Barnhart, E. & Desplan, C. Parallel Activin and BMP signaling coordinates R7/R8 photoreceptor subtype pairing in the stochastic Drosophila retina. *eLife* **6**; 10.7554/eLife.25301 (2017).

50. Maurel-Zaffran, C. & Treisman, J. E. pannier acts upstream of wingless to direct dorsal eye disc development in Drosophila. *Development* **127,** 1007–1016 (2000).

51. Pereira, P. S., Pinho, S., Johnson, K., Couso, J. P. & Casares, F. A 3' cis-regulatory region controls wingless expression in the Drosophila eye and leg primordia. *Developmental dynamics : an official publication of the American Association of Anatomists* **235,** 225–234; 10.1002/dvdy.20606 (2006).

52. Singh, A. & Choi, K.-W. Initial state of the Drosophila eye before dorsoventral specification is equivalent to ventral. *Development* **130,** 6351–6360; 10.1242/dev.00864 (2003).

53. Fear, J. M. *et al.* Buffering of Genetic Regulatory Networks in Drosophila melanogaster. *Genetics* **203,** 1177–1190; 10.1534/genetics.116.188797 (2016).

54. Cannavò, E. *et al.* Genetic variants regulating expression levels and isoform diversity during embryogenesis. *Nature* **541,** 402–406; 10.1038/nature20802 (2017).

55. Singh, A., Chan, J., Chern, J. J. & Choi, K.-W. Genetic interaction of Lobe with its modifiers in dorsoventral patterning and growth of the Drosophila eye. *Genetics* **171,** 169–183; 10.1534/genetics.105.044180 (2005).

56. Oros, S. M., Tare, M., Kango-Singh, M. & Singh, A. Dorsal eye selector pannier (pnr) suppresses the eye fate to define dorsal margin of the Drosophila eye. *Developmental Biology* **346,** 258–271; 10.1016/j.ydbio.2010.07.030 (2010).

57. García-García, M. J., Ramain, P., Simpson, P. & Modolell, J. Different contributions of pannier and wingless to the patterning of the dorsal mesothorax of Drosophila. *Development* **126,** 3523–3532 (1999).

58. Murali, T. *et al.* DroID 2011: a comprehensive, integrated resource for protein, transcription factor, RNA and gene interactions for Drosophila. *Nucleic Acids Research* **39,** D736-43; 10.1093/nar/gkq1092 (2011).

59. Yu, J., Pacifico, S., Liu, G. & Finley, R. L. DroID: the Drosophila Interactions Database, a comprehensive resource for annotated gene and protein interactions. *BMC Genomics* **9,** 461; 10.1186/1471-2164-9-461 (2008).

60. Haenlin, M. *et al.* Transcriptional activity of Pannier is regulated negatively by heterodimerization of the GATA DNA-binding domain with a cofactor encoded by the u-shaped gene of Drosophila. *Genes & Development* **11,** 3096–3108; 10.1101/gad.11.22.3096 (1997).

61. Fossett, N. *et al.* The Friend of GATA proteins U-shaped, FOG-1, and FOG-2 function as negative regulators of blood, heart, and eye development in Drosophila. *Proceedings of the National Academy of Sciences* **98,** 7342–7347; 10.1073/pnas.131215798 (2001).

62. Sorrentino, R. P., Tokusumi, T. & Schulz, R. A. The Friend of GATA protein U-shaped functions as a hematopoietic tumor suppressor in Drosophila. *Developmental Biology* **311,** 311–323; 10.1016/j.ydbio.2007.08.011 (2007).

63. Cubadda, Y. *et al.* u-shaped encodes a zinc finger protein that regulates the proneural genes achaete and scute during the formation of bristles in Drosophila. *Genes & Development* **11,** 3083–3095; 10.1101/gad.11.22.3083 (1997).

64. Wagner, G. P. & Lynch, V. J. The gene regulatory logic of transcription factor evolution. *Trends in Ecology & Evolution* **23,** 377–385; 10.1016/j.tree.2008.03.006 (2008).

65. Alvarez-Ponce, D., Aguadé, M. & Rozas, J. Network-level molecular evolutionary analysis of the insulin/TOR signal transduction pathway across 12 Drosophila genomes. *Genome Research* **19,** 234–242; 10.1101/gr.084038.108 (2009).

66. Davila-Velderrain, J., Servin-Marquez, A. & Alvarez-Buylla, E. R. Molecular evolution constraints in the floral organ specification gene regulatory network module across 18 angiosperm genomes. *Molecular Biology and Evolution* **31,** 560–573; 10.1093/molbev/mst223 (2014).

67. Halder, G., Callaerts, P. & Gehring, W. J. Induction of ectopic eyes by targeted expression of the eyeless gene in Drosophila. *Science (New York, N.Y.)* **267,** 1788–1792; 10.1126/science.7892602 (1995).

68. Carroll, S. B. Evo-devo and an expanding evolutionary synthesis: a genetic theory of morphological evolution. A Genetic Theory of Morphological Evolution. *Cell* **134,** 25–36; 10.1016/j.cell.2008.06.030 (2008).

69. Raff, R. A. Evo-devo: the evolution of a new discipline. *Nat Rev Genet* **1,** 74–79; 10.1038/35049594 (2000).

70. Laubichler, M. D. & Maienschein, J. (eds.). *From embryology to evo-devo. A history of developmental evolution* (MIT Press, Cambridge, Mass, 2010).

71. Stern, D. L. & Orgogozo, V. The loci of evolution. How predictable is genetic evolution? *Evolution* **62,** 2155–2177; 10.1111/j.1558-5646.2008.00450.x (2008).

72. Buchberger, E., Reis, M., Lu, T.-H. & Posnien, N. Cloudy with a Chance of Insights: Context Dependent Gene Regulation and Implications for Evolutionary Studies. *Genes* **10**; 10.3390/genes10070492 (2019).

73. Peter, I. & Davidson, E. H. (eds.). *Genomic Control Process. Development and Evolution* (Academic Press, 2015).

74. Peter, I. S. & Davidson, E. H. Evolution of gene regulatory networks controlling body plan development. *Cell* **144,** 970–985; 10.1016/j.cell.2011.02.017 (2011).

75. Norry, F. M., Vilardi, J. C. & Hasson, E. Negative genetic correlation between traits of the Drosophila head, and interspecific divergence in head shape. *Heredity* **85,** 177–183; 10.1046/j.1365-2540.2000.00735.x (2000).

76. Ramaekers, A. *et al.* Altering the Temporal Regulation of One Transcription Factor Drives Evolutionary Trade-Offs between Head Sensory Organs. *Developmental Cell* **50,** 780-792.e7; 10.1016/j.devcel.2019.07.027 (2019).

77. Keesey, I. W., Grabe, V., Knaden, M. & Hansson, B. S. Niche partitioning as a selective pressure for the evolution of the Drosophila nervous system. *bioRxiv* **110**; 10.1101/690529 (2019).

78. Chen, C., Zhang, D., Hazbun, T. R. & Zhang, M. Inferring Gene Regulatory Networks from a Population of Yeast Segregants. *Sci Rep* **9,** 1197; 10.1038/s41598-018-37667-4 (2019).

79. Tsuda, M. E. & Kawata, M. Evolution of gene regulatory networks by fluctuating selection and intrinsic constraints. *PLOS Computational Biology* **6**; 10.1371/journal.pcbi.1000873 (2010).

80. Thompson, D., Regev, A. & Roy, S. Comparative analysis of gene regulatory networks: from network reconstruction to evolution. *Annual Review of Cell and Developmental Biology* **31,** 399–428; 10.1146/annurev-cellbio-100913-012908 (2015).

81. Baker, L. R. *et al.* Eyeless/Pax6 initiates eye formation non-autonomously from the peripodial epithelium. *Development (Cambridge, England)* **145**; 10.1242/dev.163329 (2018).

82. Wang, L. H., Huang, Y. T., Tsai, Y. C. & Sun, Y. H. The role of eyg Pax gene in the development of the head vertex in Drosophila. *Developmental Biology* **337,** 246–258; 10.1016/j.ydbio.2009.10.038 (2010).

83. Magri, M. S., Domínguez-Cejudo, M. A. & Casares, F. Wnt controls the medial-lateral subdivision of the Drosophila head. *Biology letters* **14**; 10.1098/rsbl.2018.0258 (2018).

84. Fromental-Ramain, C., Taquet, N. & Ramain, P. Transcriptional interactions between the pannier isoforms and the cofactor U-shaped during neural development in Drosophila. *Mechanisms of Development* **127,** 442–457; 10.1016/j.mod.2010.08.002 (2010).

85. Fromental-Ramain, C., Vanolst, L., Delaporte, C. & Ramain, P. pannier encodes two structurally related isoforms that are differentially expressed during Drosophila development and display distinct functions during thorax patterning. *Mechanisms of Development* **125,** 43–57; 10.1016/j.mod.2007.10.008 (2008).

86. Heitzler, P., Haenlin, M., Ramain, P., Calleja, M. & Simpson, P. A genetic analysis of pannier, a gene necessary for viability of dorsal tissues and bristle positioning in Drosophila. *Genetics* **143,** 1271–1286 (1996).

87. Gómez-Skarmeta, J. L., Campuzano, S. & Modolell, J. Half a century of neural prepatterning: the story of a few bristles and many genes. The story of a few bristles and many genes. *Nature reviews. Neuroscience* **4,** 587–598; 10.1038/nrn1142 (2003).

88. Ramain, P., Heitzler, P., Haenlin, M. & Simpson, P. pannier, a negative regulator of achaete and scute in Drosophila, encodes a zinc finger protein with homology to the vertebrate transcription factor GATA-1. *Development* **119,** 1277–1291 (1993).

89. Huang, F., Dambly-Chaudière, C. & Ghysen, A. The emergence of sense organs in the wing disc of Drosophila. *Development* **111,** 1087–1095 (1991).

90. Vermeirssen, V. *et al.* Transcription factor modularity in a gene-centered C. elegans core neuronal protein-DNA interaction network. *Genome Research* **17,** 1061–1071; 10.1101/gr.6148107 (2007).

91. Borneman, A. R. *et al.* Target hub proteins serve as master regulators of development in yeast. *Genes & Development* **20,** 435–448; 10.1101/gad.1389306 (2006).

92. Promislow, D. A regulatory network analysis of phenotypic plasticity in yeast. *The American naturalist* **165,** 515–523; 10.1086/429161 (2005).

93. Potier, D. *et al.* Mapping gene regulatory networks in Drosophila eye development by large-scale transcriptome perturbations and motif inference. *Cell Reports* **9,** 2290–2303; 10.1016/j.celrep.2014.11.038 (2014).

94. Lopes, C. S. & Casares, F. Hth maintains the pool of eye progenitors and its downregulation by Dpp and Hh couples retinal fate acquisition with cell cycle exit. *Developmental Biology* **339,** 78–88; 10.1016/j.ydbio.2009.12.020 (2010).

95. Bessa, J., Gebelein, B., Pichaud, F., Casares, F. & Mann, R. S. Combinatorial control of Drosophila eye development by eyeless, homothorax, and teashirt. *Genes & Development* **16,** 2415–2427; 10.1101/gad.1009002 (2002).

96. Palliyil, S. *et al.* Allocation of distinct organ fates from a precursor field requires a shift in expression and function of gene regulatory networks. *PLoS Genetics* **14,** e1007185; 10.1371/journal.pgen.1007185 (2018).

97. Lachaise, D., David, J. R., Lemeunier, F. & Tsacas, L. The reproductive relationships of *Drosophila sechellia* with *D. mauritiana*, *D. simulans*, and *D. melanogaster* from the Afrotropical region. *Evolution* **40,** 262–271 (1986).

98. Stern, D. L. Identification of loci that cause phenotypic variation in diverse species with the reciprocal hemizygosity test. *Trends in Genetics* **30,** 547–554; 10.1016/j.tig.2014.09.006 (2014).

99. Torres-Oliva, M., Almudi, I., McGregor, A. P. & Posnien, N. A robust (re-)annotation approach to generate unbiased mapping references for RNA-seq-based analyses of differential expression across closely related species. *BMC Genomics* **17,** 392; 10.1186/s12864-016-2646-x (2016).

100. Langmead, B. & Salzberg, S. L. Fast gapped-read alignment with Bowtie 2. *Nat Methods* **9,** 357–359; 10.1038/nmeth.1923 (2012).

101. Li, H. *et al.* The Sequence Alignment/Map format and SAMtools. *Bioinformatics* **25,** 2078–2079; 10.1093/bioinformatics/btp352 (2009).

102. Li, H. A statistical framework for SNP calling, mutation discovery, association mapping and population genetical parameter estimation from sequencing data. *Bioinformatics* **27,** 2987–2993; 10.1093/bioinformatics/btr509 (2011).

103. Love, M. I., Huber, W. & Anders, S. Moderated estimation of fold change and dispersion for RNA-seq data with DESeq2. *(Keine Angabe)* **15,** 550; 10.1186/s13059-014-0550-8 (2014).

104. Zhu, A., Ibrahim, J. G. & Love, M. I. Heavy-tailed prior distributions for sequence count data: removing the noise and preserving large differences. *Bioinformatics* **35,** 2084–2092; 10.1093/bioinformatics/bty895 (2019).

105. Zhou, Y. *et al.* Metascape provides a biologist-oriented resource for the analysis of systems-level datasets. *Nature Communications* **10,** 1523; 10.1038/s41467-019-09234-6 (2019).

106. Godichon-Baggioni, A., Maugis-Rabusseau, C. & Rau, A. Clustering transformed compositional data using K -means, with applications in gene expression and bicycle sharing system data. *Journal of Applied Statistics* **46,** 47–65; 10.1080/02664763.2018.1454894 (2019).

107. Rau, A. & Maugis-Rabusseau, C. Transformation and model choice for RNA-seq co-expression analysis. *Briefings in bioinformatics* **19,** 425–436; 10.1093/bib/bbw128 (2018).

108. Imrichová, H., Hulselmans, G., Atak, Z. K., Potier, D. & Aerts, S. i-cisTarget 2015 update. Generalized cis-regulatory enrichment analysis in human, mouse and fly. *Nucleic Acids Research* **43,** W57-64; 10.1093/nar/gkv395 (2015).

109. Herrmann, C., van de Sande, B., Potier, D. & Aerts, S. i-cisTarget. An integrative genomics method for the prediction of regulatory features and cis-regulatory modules. *Nucleic Acids Research* **40,** e114-e114; 10.1093/nar/gks543 (2012).

110. Thurmond, J. *et al.* FlyBase 2.0: the next generation. *Nucleic Acids Research* **47,** D759-D765; 10.1093/nar/gky1003 (2019).

111. Buenrostro, J. D., Giresi, P. G., Zaba, L. C., Chang, H. Y. & Greenleaf, W. J. Transposition of native chromatin for fast and sensitive epigenomic profiling of open chromatin, DNA-binding proteins and nucleosome position. *Nature Methods* **10,** 1213–1218; 10.1038/nmeth.2688 (2013).

112. Bolger, A. M., Lohse, M. & Usadel, B. Trimmomatic: a flexible trimmer for Illumina sequence data. *Bioinformatics* **30,** 2114–2120; 10.1093/bioinformatics/btu170 (2014).

113. Zhang, Y. *et al.* Model-based analysis of ChIP-Seq (MACS). *Genome Biology* **9,** R137; 10.1186/gb-2008-9-9-r137 (2008).

114. Freese, N. H., Norris, D. C. & Loraine, A. E. Integrated genome browser: visual analytics platform for genomics. *Bioinformatics* **32,** 2089–2095; 10.1093/bioinformatics/btw069 (2016).

115. Heinz, S. *et al.* Simple Combinations of Lineage-Determining Transcription Factors Prime cis-Regulatory Elements Required for Macrophage and B Cell Identities. *Molecular Cell* **38,** 576–589; 10.1016/j.molcel.2010.05.004 (2010).

116. Junion, G. *et al.* A transcription factor collective defines cardiac cell fate and reflects lineage history. *Cell* **148,** 473–486; 10.1016/j.cell.2012.01.030 (2012).

117. Shannon, P. *et al.* Cytoscape. A software Environment for integrated models of biomolecular interaction networks. *Genome Research* **13,** 2498–2504; 10.1101/gr.1239303 (2003).

118. Rohlf, F. The tps series of software. *Hystrix, the Italian Journal of Mammalogy* **26**; 10.4404/hystrix-26.1-11264 (2015).

119. Klingenberg, C. P. MorphoJ. An integrated software package for geometric morphometrics. *Molecular Ecology Resources* **11,** 353–357; 10.1111/j.1755-0998.2010.02924.x (2011).

120. Calleja, M., Moreno, E., Pelaz, S. & Morata, G. Visualization of gene expression in living adult Drosophila. *Science* **274,** 252–255; 10.1126/science.274.5285.252 (1996).

121. Struhl, G. & Basler, K. Organizing activity of wingless protein in Drosophila. *Cell* **72,** 527–540; 10.1016/0092-8674(93)90072-X (1993).

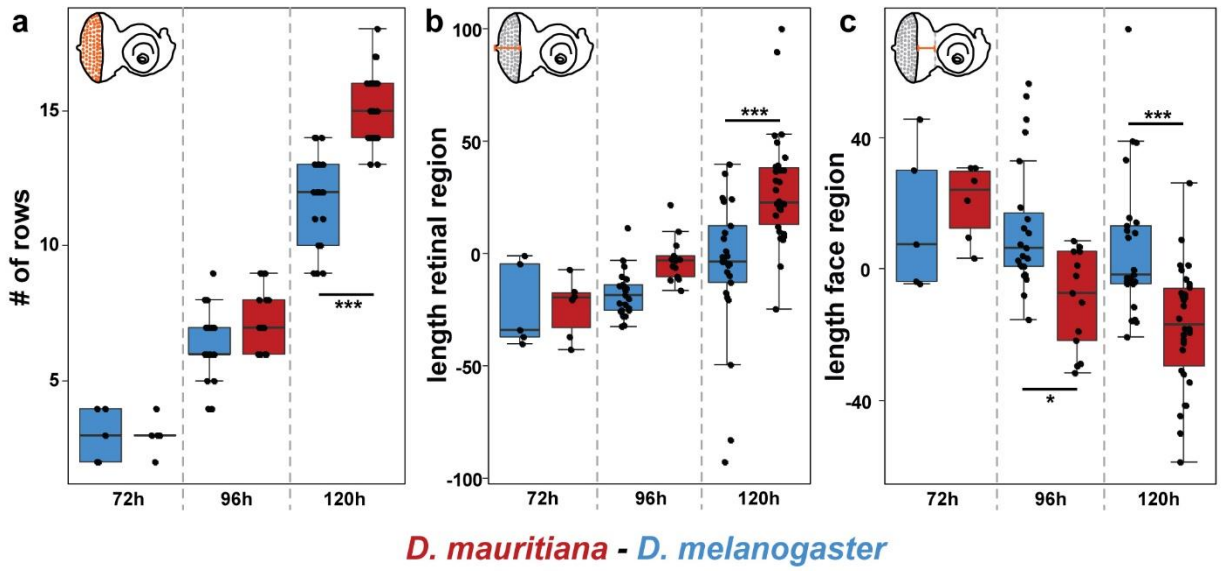

Figure S1 | Quantitative comparative analysis of eye-antennal disc development in *D. melanogaster* and *D. mauritiana* reveals trade-off between retinal interstitial cuticle anlagen. a, Number of ommatidial precursor rows was counted along the equator region of the eye-antennal disc. Significant differences were observed at 120 h after egg laying (AEL) ($F_{5,96} = 210.8$, $p < 2e^{-16}$). **b**, Distance from the optic stalk to the morphogenetic furrow was measured along the equator region. Significant differences were observed at 120 h AEL ($F_{5,96} = 15.61$, $p = 3.2e^{-11}$). **c**, Distance from the morphogenetic furrow to the antennal anlagen was measured. From 96 h AEL on, we observed significant differences ($F_{5,96} = 10.23$, $p = 7e^{-8}$). One-way ANOVA followed by Tukey multiple comparisons: *** <0.001; * 0.01248.

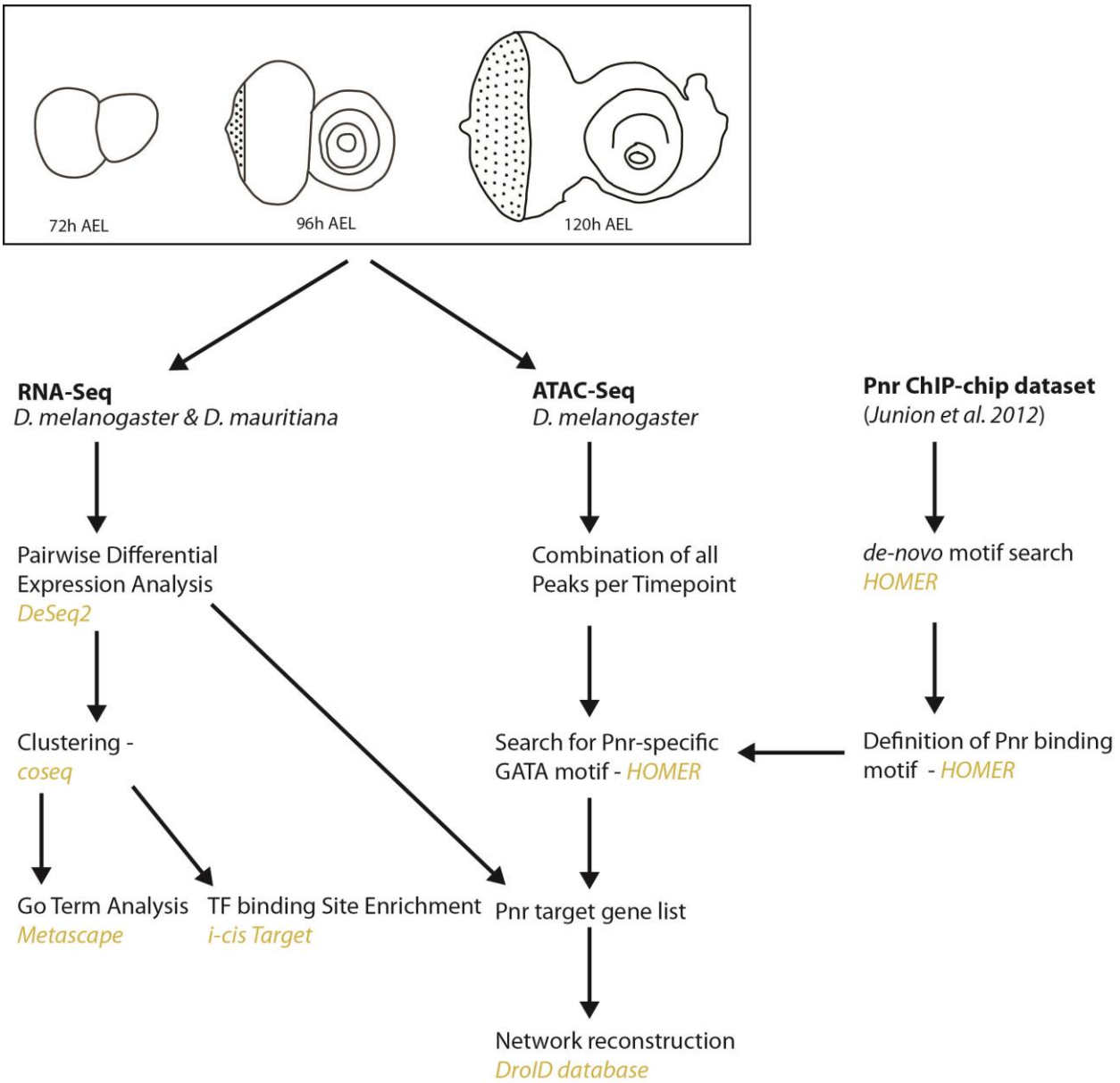

Figure S2 | Overview of RNAseq and ATACseq analyses. Scheme of the datasets generated and used for the analysis, together with the analysis pipeline. We generated RNA-seq and ATAC-seq datasets of developing eye-antennal discs at three stages at late-L2, mid-L3 and late L3 (72h AEL (after egg laying), 96h AEL and 120h AEL). The arrows outline the analysis pipeline and programs used in each step are given in yellow.

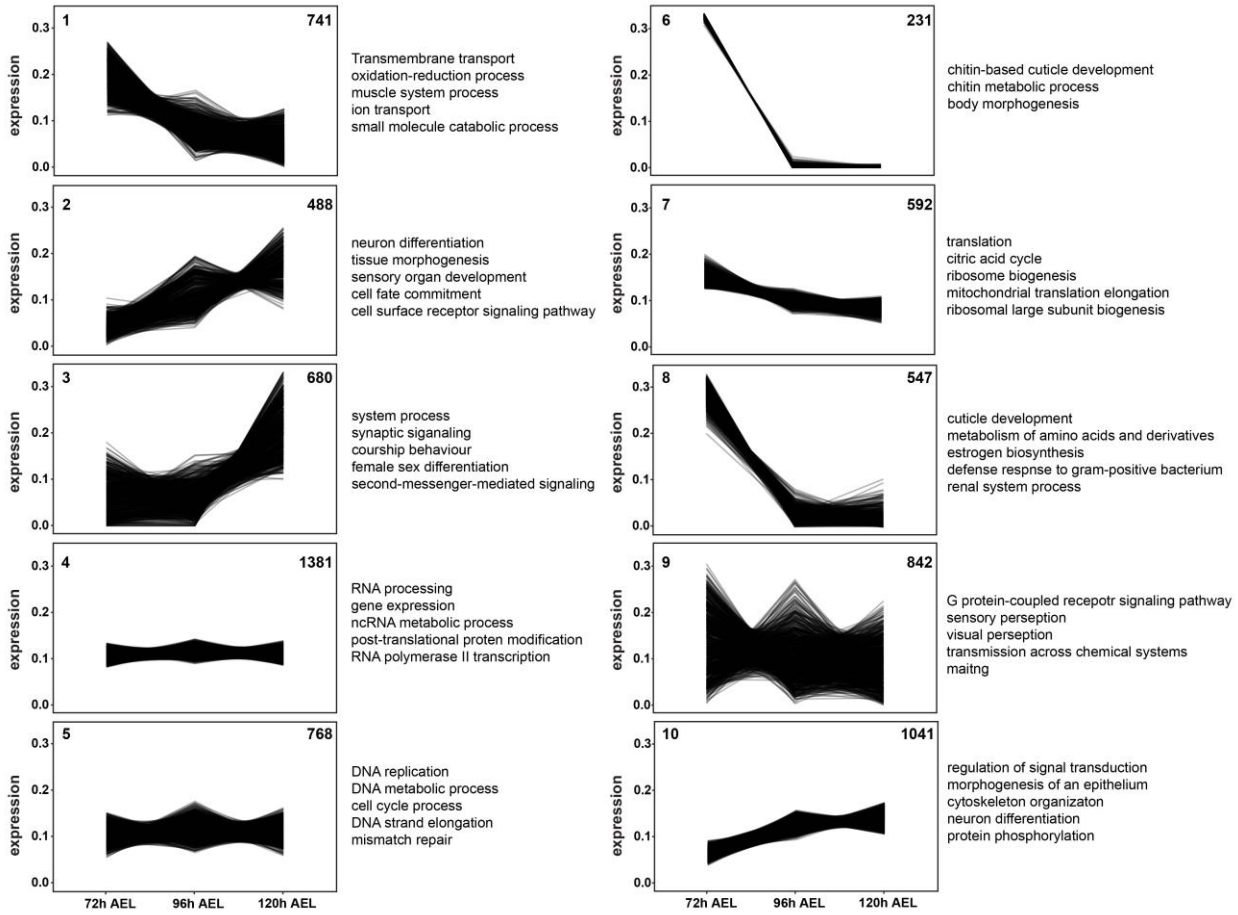

Figure S3 | Clustering of genes that showed conserved expression between *D. melanogaster* and *D. mauritiana*. Conserved genes were clustered based on expression dynamics across the three stages and a GO enrichment analysis was performed for each cluster. The number of genes in each cluster is given in the top right corner. Genes that were upregulated at early stages or constantly expressed over the three time-points, are mainly enriched in metabolic processes, cell-cycle processes and gene expression (e.g. clusters 4, 5 and 7). This is consistent with the fact, that the developing eye-antennal disc is a highly proliferative and growing tissue [1]. Genes that were highly expressed at 72h AEL and barely expressed at the two later stages, are enriched in cuticle development (e.g. clusters 6 and 8), reflecting the moulting of the *Drosophila* larva at the end of the 2nd instar. Genes that got steadily upregulated at the two later stages are mainly enriched in neuronal processes (e.g. clusters 2,3 and 10), consistent with the ongoing differentiation of ommatidia at these time-points [2].

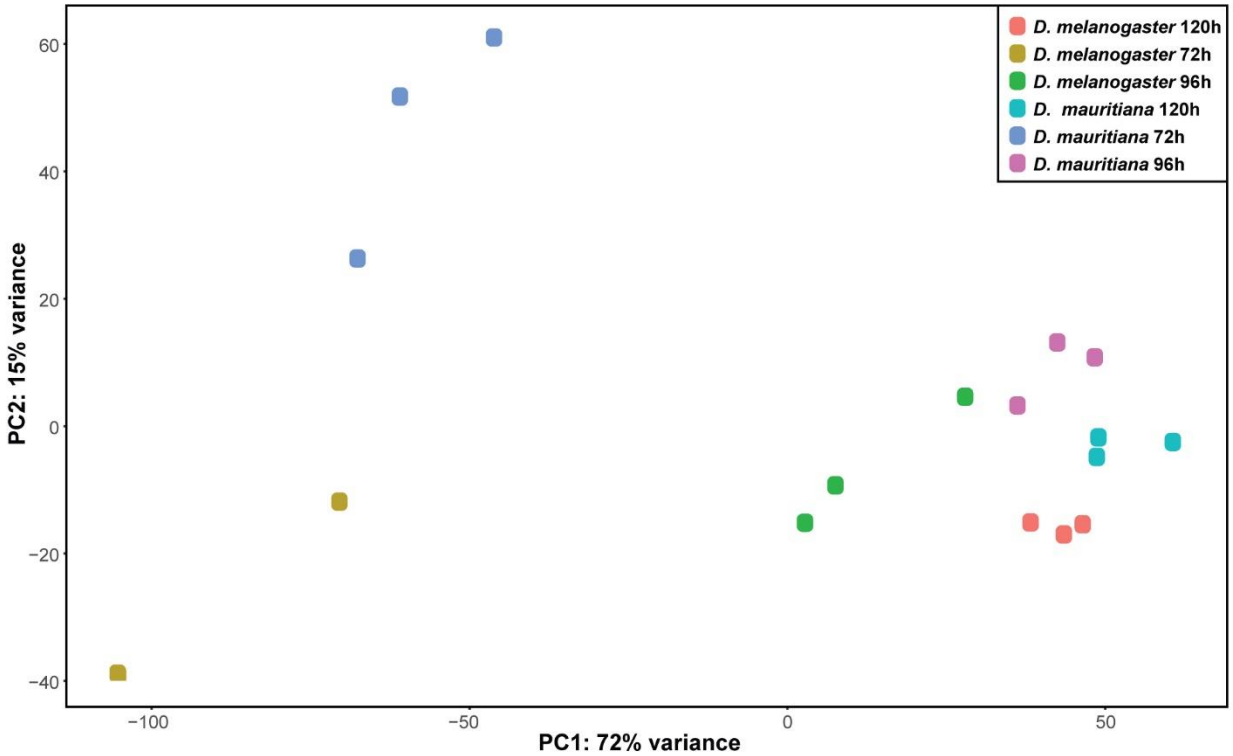

Figure S4 | Principal Component Analyses of all RNAseq samples. Analysis is based on rlog transformed read counts. PC1 separates the samples according to time-points, whereas PC2 separates them mainly the by species.

a

possibleTFs	NES
pnr	7.13
nejire	5.71
Pmad	4.75
mef2	3.43

b

Cluster_Number	ClusterSize	pnr_enriched?_Rank	NES	OverlapHCL	OverlapHCL%
1	272	137	3.1	3	1%
2	458	94	3.4	8	2%
3	354	61	3.5	5	1%
4	488	-	-	42	9%
5	224	-	-	1	0%
6	508	-	-	10	2%
7	582	33	4.4	15	3%
8	804	11	6.9	76	9%
9	488	31	9.5	60	12%
10	346	-	-	10	3%
11	654	-	-	89	14%
12	392	-	-	10	3%
13	912	70	5.2	215	24%
14	1499	3	18.9	168	11%
15	369	209	3.1	4	1%

c

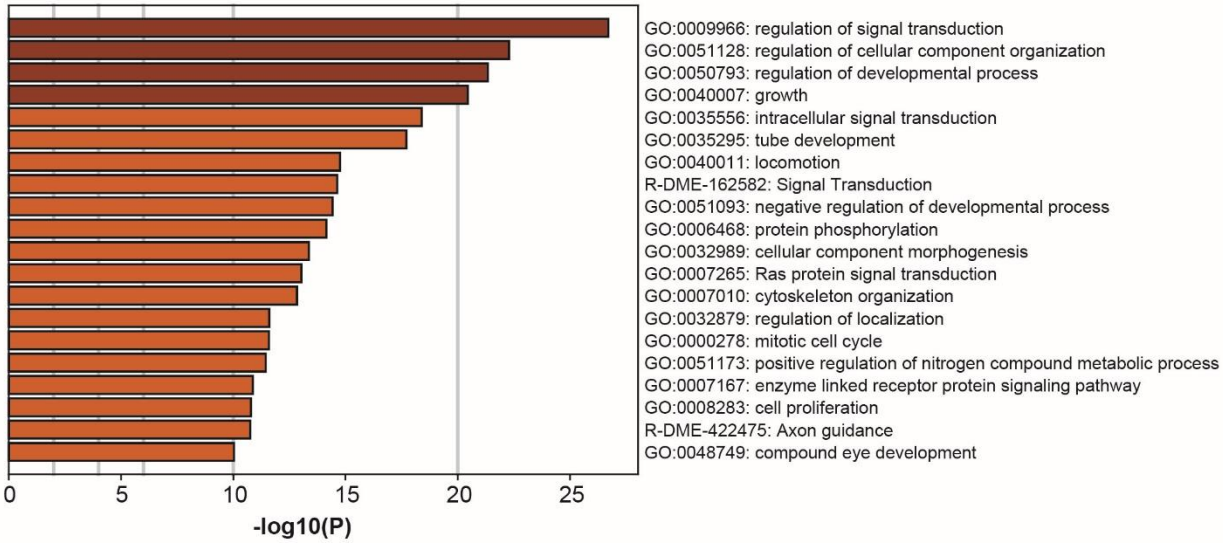

Figure S5 | Cross validation of putative direct Pnr target genes. a, Transcription factor binding site enrichment in 5kb upstream of the transcription start site, 5'UTR regions and 1st introns of all predicted Pnr target genes (NES-values represent enrichment score). The identification of putative pMad target genes among Pnr targets may confirm the previous observation that both proteins interact physically during larval development [3]. **b,** Table showing the number of DEGs clustered together, and if available, enrichment of the Pnr motif based on i-cis Target, together with the NES score. The last two columns show the overlap between the predicted Pnr target gene list and the respective cluster. **c,** GO-term enrichment analysis of all predicted Pnr target genes. Enrichment in processes such as signal transduction, growth, cell cycle but also in more specific terms like compound eye development were identified.

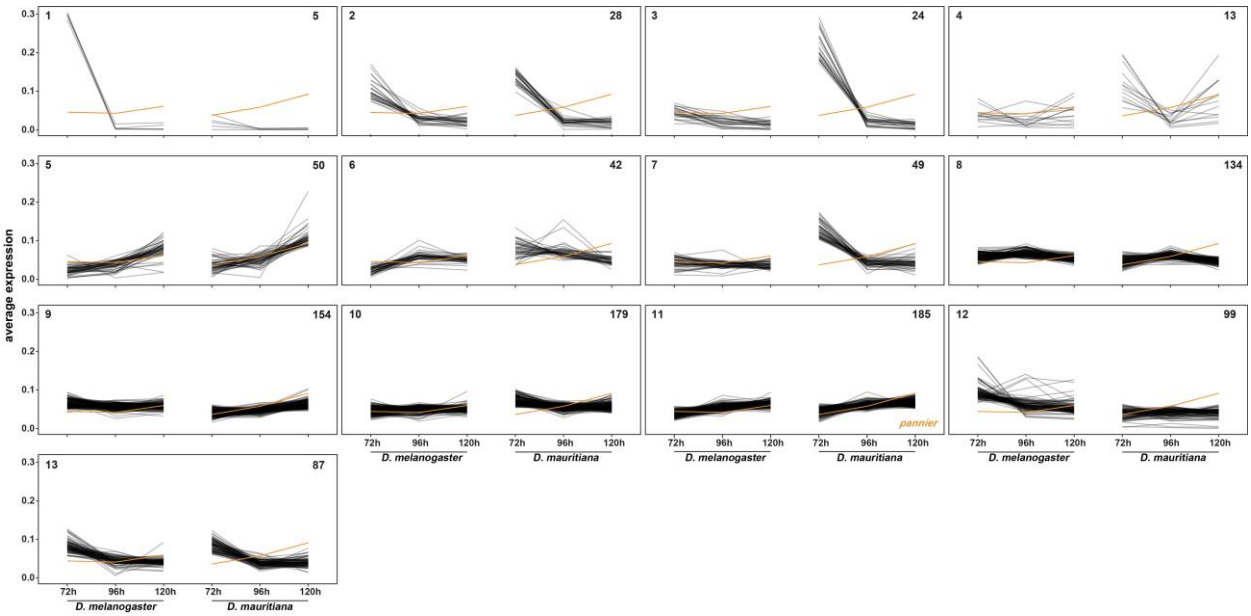

Figure S6 | Clustering of differentially expressed putative Pnr target genes based on expression dynamics. The number of genes in each cluster is provided in the top right corner. Among the 13 obtained clusters, *pnr* itself is present in cluster 11. The expression profile of *pnr* is provided in orange in each cluster for comparison. While other genes in cluster 11, as well as genes in clusters 5, 9 and 10 showed the same expression dynamics as *pnr*, genes in other clusters showed the exact opposite trend. For instance, the Pnr target genes in cluster 3 were highly expressed at 72 h AEL in *D. mauritiana*, while *pnr* itself showed a relatively low expression. The expression of the same target genes decreased at 120 h AEL with *pnr* expression increasing at the same time. This contrasting expression profile strongly suggests that those target genes may be repressed by Pnr action. In contrast, genes in clusters that show the same dynamics as *pnr* may be positively regulated by Pnr.

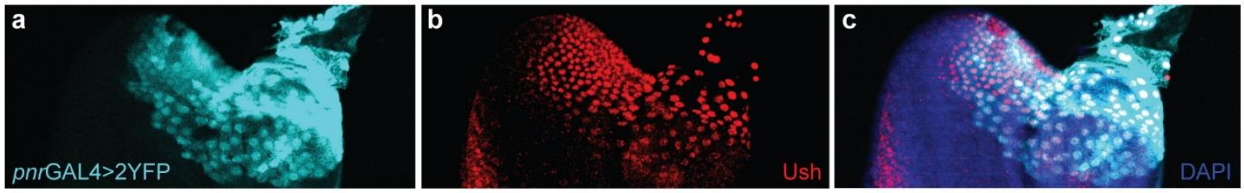

Figure S7 | Co-expression of *pnr* and Ush in the peripodial membrane of the eye-antennal disc in *D. melanogaster*. **a,** *pnr* expression visualized by *pnr*GAL4>2YFP reporter line. **b,** Ush protein localization detected with an α-Ush antibody. **c,** Overlay of **a** and **b**. Posterior to the left and dorsal up.

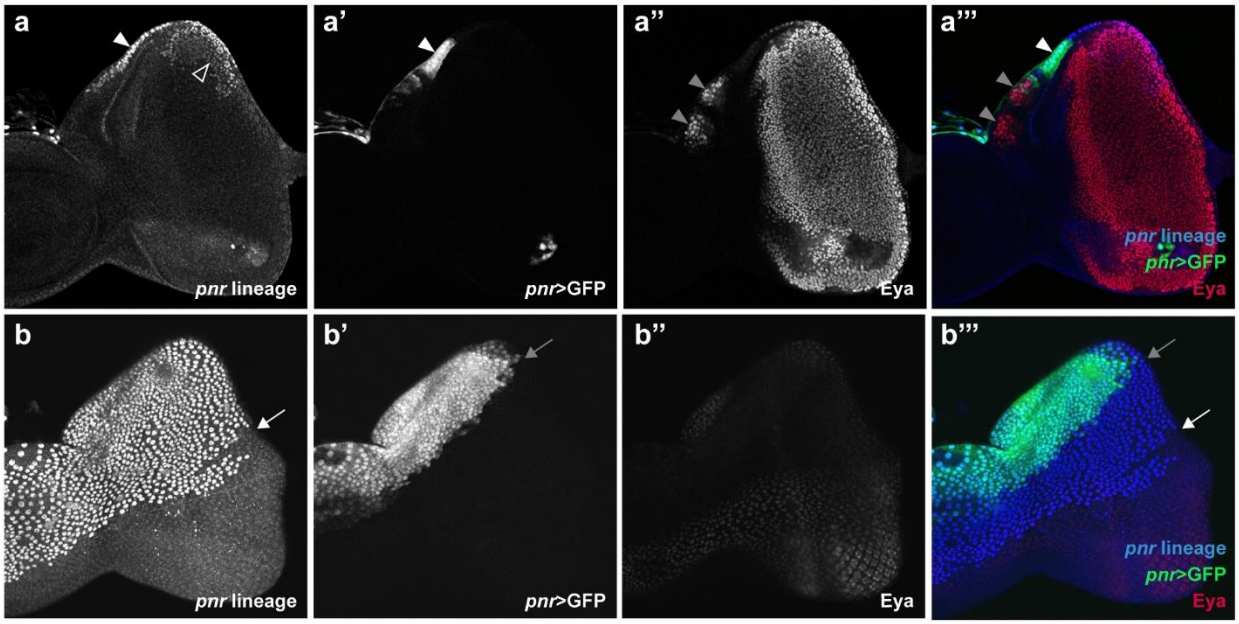

Figure S8 | Lineage of *pnr*-expressing cells in the developing eye-antennal disc. a-a''', Confocal scan on the level of the disc proper. Cells of the *pnr* lineage contribute to the dorsal disc margin (white arrowheads). A few cells of the *pnr*-lineage also contributed to the dorsal-posterior developing retinal field (open arrowheads). *pnr*>GFP expression can be detected in the margin cells (white arrowheads) posterior to the ocelli anlagen (grey arrowheads). **b-b''',** Confocal scan on the level of the peripodial epithelium. Cells of the *pnr* lineage covered most of the dorsal part of the peripodial epithelium (white arrow), while *pnr* expression is restricted to the dorsal most region (grey arrow) in late L3 larval stages.

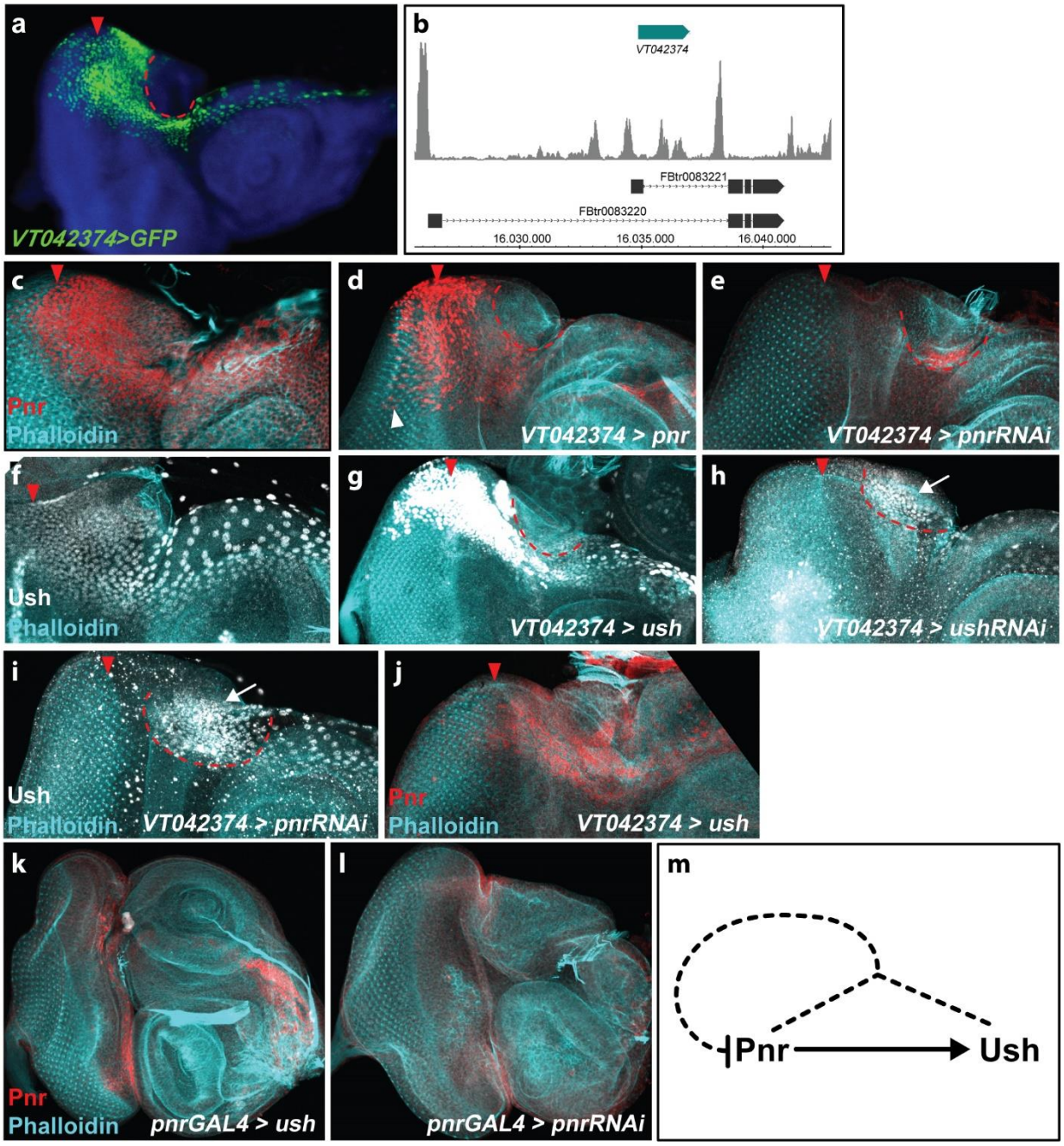

Figure S9 | Genetic interactions of *pnr* and *ush* in *D. melanogaster*. a, The VT042374 lines drives expression of GFP in the dorsal peripodial epithelium. Note that the line does not drive expression in the ocelli region (red dotted line), where endogenous Pnr expression is weaker (compare to **c**). Furthermore, the GFP expression extends more posteriorly beyond the morphogenetic furrow (red arrowhead) compared to the wildtype protein expression of Pnr (compare to **c**). **b,** Analysis of the *pnr* locus showed that the enhancer fragment of the VT042374 line overlaps with open chromatin (ATACseq peaks; grey) regions in the first intron, strongly suggesting that partial endogenous *pnr* expression is reported. **c,** Wildtype Pnr expression detected with anti-Pnr antibody. **d,** Overexpression of *pnr* with the VT042374 line leads to ectopic expression of Pnr posterior to the morphogenetic furrow (white arrowhead). **e,** *pnr* RNAi knockdown with

the VT042374 line resulted in strong reduction of Pnr expression. **f,** Wildtype expression of Ush detected with anti-Ush antibody. **g,** Overexpression of *ush* with the VT042374 line leads to increased expression of Ush as well as ectopic expression posterior to the morphogenetic furrow. **h,** ush RNAi knockdown with the VT042374 line resulted in strong reduction of Ush expression in most of the dorsal peripodial membrane except for the ocellar region, where the VT042374 line does not drive expression (white arrow). **i,** Knockdown of *pnr* resulted in reduction of Ush expression, except for the ocellar region, where the VT042374 line does not drive expression (white arrow). **j,** Overexpression of *ush* resulted in reduction of Pnr expression. **k,** Overexpression of *ush* resulted in duplication of antennae anlagen. **l,** Knockdown of *pnr* resulted in duplication of antennae anlagen. **m,** Summary of putative regulatory interactions between *pnr* and *ush*.

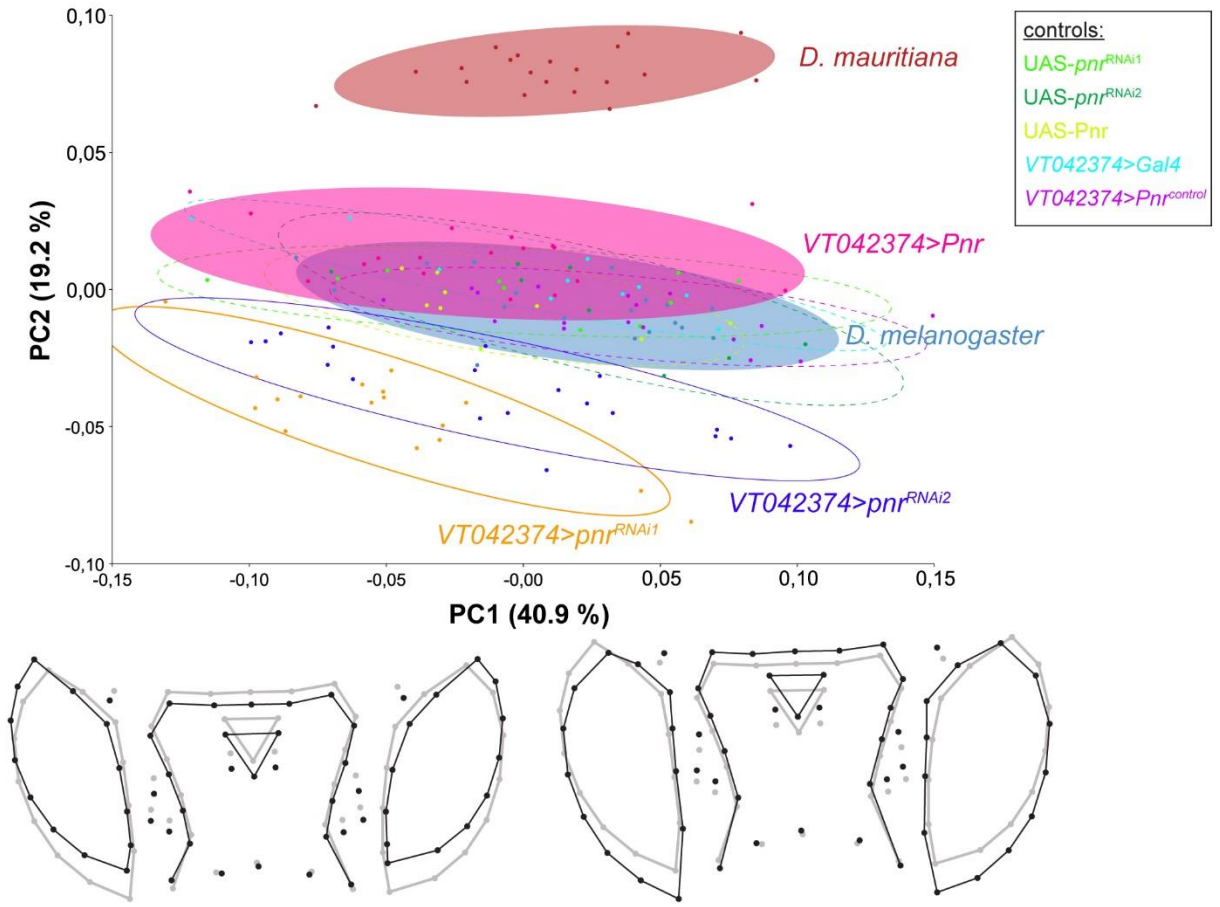

Figure S10 | Principal Component Analysis showing artificial shape changes due to variation in positioning of the heads during image acquision. PC1 captured up- and down facing heads (see shape outlines representing -0.1 and 0.1 along PC1). Since this effect is present across all samples, this positioning artefact affects all samples simultaneously. We excluded the first principal component (PC1) and analyzed PC2 and PC3 in more detail.

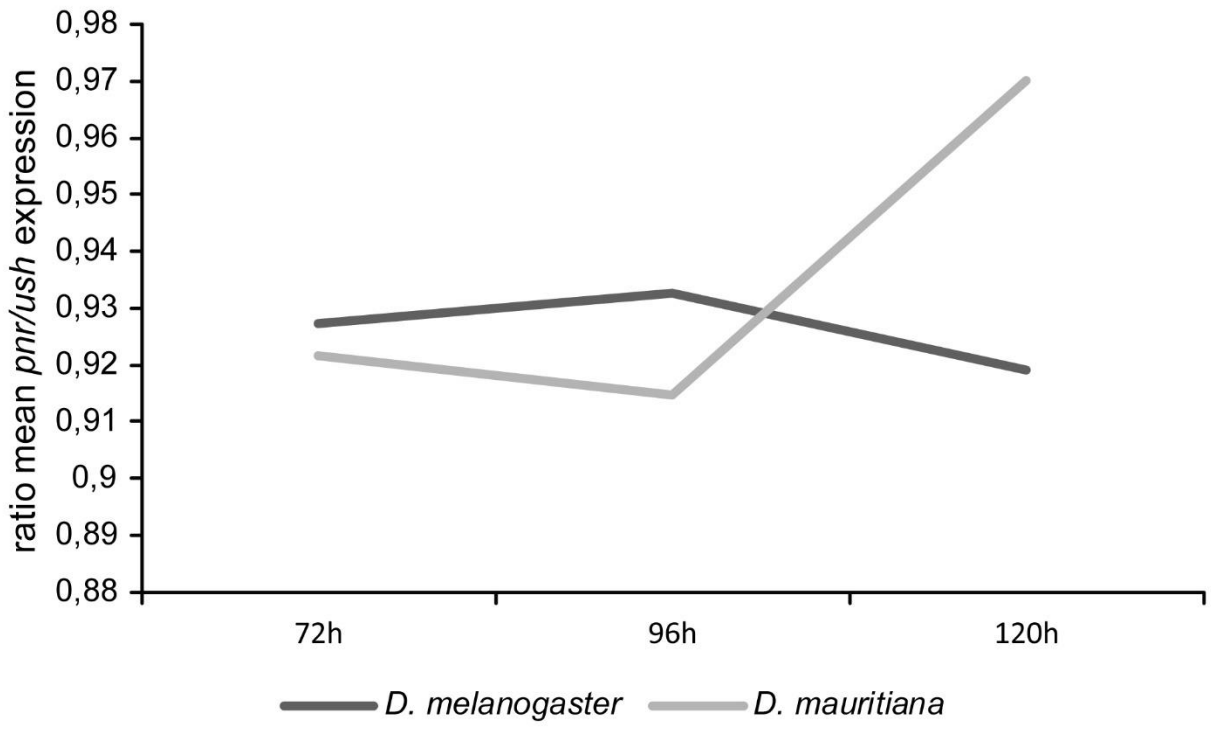

Figure S11 | Ratio of mean expression of *pnr* and *ush* in *D. melanogaster* and *D. mauritiana*.

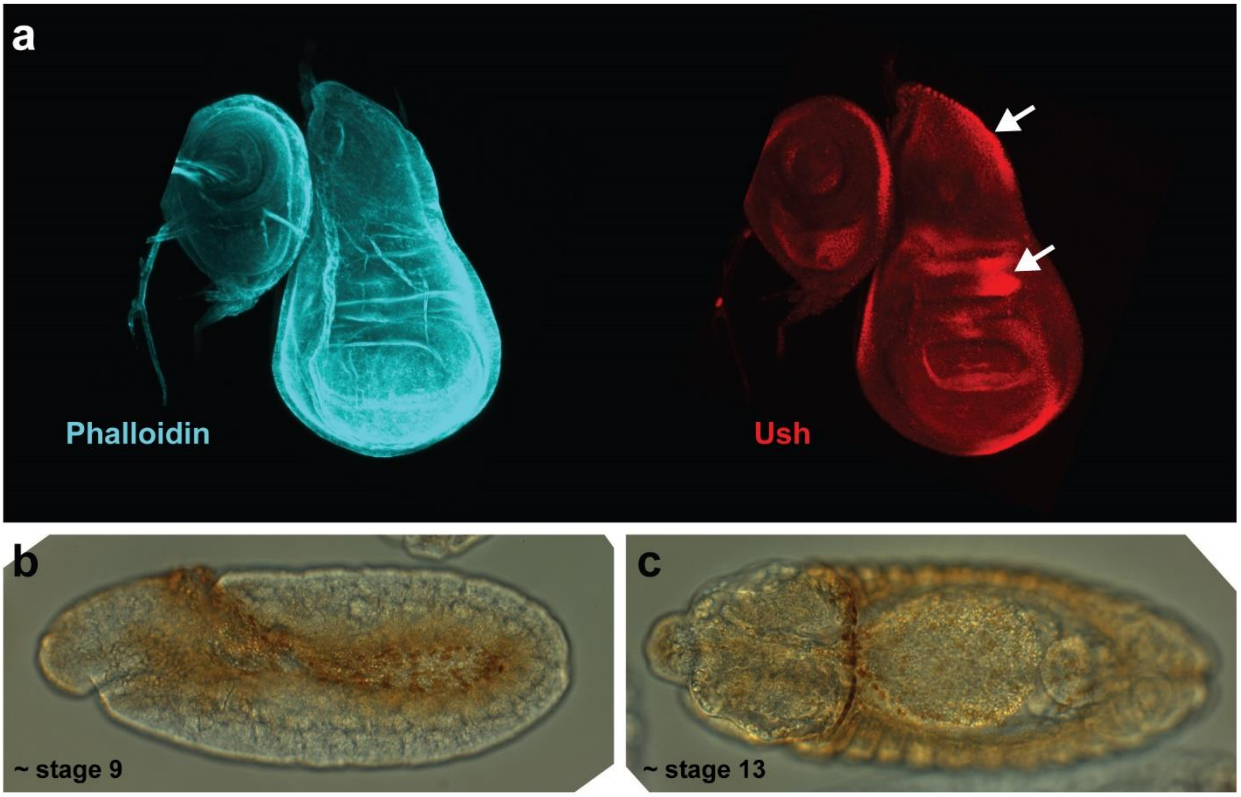

Figure S12 | Expression of Ush in the wing imaginal disc and in the embryo. a, Ush protein location in the developing *Drosophila* wing disc, detected with the newly generated α-Ush antibody. The regions where Ush were detected in this tissue (white arrows) are reminiscent of the regions, where *ush* mRNA can be detected using *in-situ* hybridization as shown in [4]. **b,** Ush protein location in a developing *Drosophila* embryo at about stage 9, detected with the α-Ush antibody. Ush can be detected in the dorsal ectoderm and the head mesoderm, where also *ush* mRNA was detected, as shown in [5–8]. **c,** Ush protein location in a developing *Drosophila* embryo around ~stage 13 in the leading cells of the future dorsal closure (also compare to *ush* mRNA in embryos stage 13-16 in [6–8]), detected with the α-Ush antibody.

Table S1 | Number of differentially expressed genes (DEGs).

stage	upregulated in *D. melanogaster*	upregulated in *D. mauritiana*	total number of DEGs
72h AEL	3,244	3,439	6,683
96h AEL	1,622	1,638	3,260
120h AEL	1,130	1,250	2,380

Table S2 | GO enrichment and iCis-Target analyses for clusters of differentially expressed genes.

See Excel file Table S2

Table S3 | List of putative Pnr target genes.

See Excel file Table S3

References

1. Kumar, J. P. My what big eyes you have. How the Drosophila retina grows. *Developmental Neurobiology* **71,** 1133–1152; 10.1002/dneu.20921 (2011).
2. .Cagan, R. in *Tissue remodeling and epithelial morphogenesis,* edited by T. Lecuit (Academic Press, San Diego, Calif., 2009), pp. 115–135.
3. Kim, A.-R., Choi, E.-B., Kim, M.-Y. & Choi, K.-W. Angiotensin-converting enzyme Ance is cooperatively regulated by Mad and Pannier in Drosophila imaginal discs. *Scientific Reports* **7,** 13174; 10.1038/s41598-017-13487-w (2017).
4. Tomoyasu, Y., Ueno, N. & Nakamura, M. The Decapentaplegic morphogen gradient regulates the notal wingless expression through induction of pannier and u-shaped in Drosophila. *Mechanisms of Development* **96,** 37–49; 10.1016/S0925-4773(00)00374-9 (2000).
5. Fossett, N. & Schulz, R. A. Conserved Cardiogenic Functions of the Multitype Zinc-Finger Proteins. *Trends in Cardiovascular Medicine* **11,** 185–190; 10.1016/S1050-1738(01)00092-5 (2001).
6. Hammonds, A. S. *et al.* Spatial expression of transcription factors in Drosophila embryonic organ development. *Genome Biol* **14,** R140; 10.1186/gb-2013-14-12-r140 (2013).
7. Tomancak, P. *et al.* Systematic determination of patterns of gene expression during Drosophila embryogenesis. *Genome Biol* **3,** RESEARCH0088; 10.1186/gb-2002-3-12-research0088 (2002).
8. Tomancak, P. *et al.* Global analysis of patterns of gene expression during Drosophila embryogenesis. *Genome Biol* **8,** R145; 10.1186/gb-2007-8-7-r145 (2007).